THE UNIVERSITY OF CALGARY

A New Method of Deconvolution Unmasks Reservoir Pressure Response of Varying Rate Drawdown Tests

by

Granger James Low

A THESIS

SUBMITTED TO THE FACULTY OF GRADUATE STUDIES

IN PARTIAL FULFILLMENT OF THE REQUIREMENTS FOR THE

DEGREE OF

MASTER OF ENGINEERING

DEPARTMENT OF

CHEMICAL AND PETROLEUM ENGINEERING

CALGARY, ALBERTA

MARCH, 1992

ISBN 0-315-75274-2

UNIVERSITY OF CALGARY

FACULTY OF GRADUATE STUDIES

The undersigned certify that they have read, and recommend to the Faculty of Graduate Studies for acceptance, a thesis entitled, "A New Method of Deconvolution Unmasks Reservoir Pressure Response of Varying Rate Drawdown Tests" submitted by Granger James Low in partial fulfillment of the requirements for the degree of Master of Engineering.

Dr. J. Stanislav (Supervisor)
Department of Chemical & Petroleum Engineering

Dr. J.D.M. Belgrave
Department of Chemical & Petroleum Engineering

Dr. M. Epstein
Department of Mechanical Engineering

Dr. A. Jeje
Department of Chemical & Petroleum Engineering

Mr. L. Mattar
Fekete Associates Inc.

April 6, 1992

Abstract

In the petroleum industry, the economic advantage of drawdown testing have long been recognized over those of buildup testing. However, drawdown tests are rarely analyzed due to the difficulty in achieving a constant production rate. Theoretically, deconvolution can make drawdown tests interpretable by unmasking reservoir response during varying rate drawdown tests. When the mathematical form of the flow rate schedule is complex or discontinuous, analog deconvolution methods become difficult to apply to well tests. Other deconvolution methods proposed in the literature to date have been unsuccessful in deconvolving all flow schedules and all flow patterns. In this thesis a new method of deconvolution is derived by using forward differences. The method requires bottom hole pressure and sandface flow rate data sampled at equal time intervals. The deconvolution method was tested with synthetic variable rate well tests convolved using four flow patterns and five sandface flow rate schedules. The flow patterns included radial flow, linear flow and spherical flow and a combination of radial and linear flow. Constant, linear, exponential, periodic and discontinuous sandface flow schedules were considered. The deconvolution algorithm was also successfully tested against two variable rate well test examples in the literature. The proposed method successfully deconvolved all synthetic well tests. In each case, the

deconvolved pressure response was similar to the original pressure influence function by the standard type curve matching. In addition, the proposed method produced reservoir parameters that matched those published for the two well tests from the literature. The deconvolution method is general in nature and applicable to all reservoir flow patterns and all sandface flow rate schedules. Use of the method improved confidence in calculated permeability and skin values. It also enables drawdown tests affected by variable flow rates to be analyzed.

Table of Contents

Table of Contents (continued)

Table of Tables

Table of Figures

Table of Figures (continued)

Nomenclature

Variable	Description	(Units)
B	formation volume factor	(rbbl/STB)
c_f	fluid compressibility	(1/psi)
c_t	total compressibility	(1/psi)
g	acceleration due to gravity	(ft/s^2)
h	formation height	(ft)
i	time counter	
k	permeability	(mD)
K	inverse Laplace transform related to the dimensionless flow rate	
k_r	radial permeability	(mD)
k_s	spherical permeability	(mD)
k_z	vertical permeability	(mD)
L	characteristic half length of a fracture	(ft)
$\mathcal{L}^{-1}$	inverse Laplace operator	
m	slope	(1/psi)
N	number of data points	
p_{1hr}	bottom hole pressure after 1 hour of flow	(psi)

Nomenclature (continued)

Variable	Description	(Units)
$\hat{p}_{1hr}$	deconvolved bottom hole pressure after 1 hour of flow	(psi)
p_D	pressure influence function or dimensionless pressure function	
p'_D	semi-log derivative of the pressure influence function (ie. $t_D \cdot dp_D/dt_D$)	
p''_D	second derivative of the pressure influence function	
p_i	initial reservoir pressure	(psi)
p_{wd}	difference between initial reservoir pressure and flowing bottom hole pressure	(psi)
$\hat{p}_{wd}$	difference between initial reservoir pressure and deconvolved flowing bottom hole pressure	(psi)
p_{wD}	dimensionless bottom hole pressure function	
p_{wDRef}	dimensionless bottom hole pressure function at a reference flow rate	

Nomenclature (continued)

Variable	Description	(Units)
p'_{wDRef}	semi-log derivative of the dimensionless bottom hole pressure function at a reference flow rate	
p_{wf}	bottom hole flowing pressure	(psi)
$\hat{p}_{wf}$	deconvolved bottom hole flowing pressure	(psi)
q	flow rate	(bbl/d)
q_D	dimensionless flow rate	
$\overline{q}_D$	average dimensionless flow rate	
q_{D1}	flow rate at time 1	(bbl/d)
q_{D2}	flow rate at time 2	(bbl/d)
q_{Di}	flow rate at time i	(bbl/d)
q_{Ref}	reference flow rate	(bbl/d)
q_{sf}	sandface flow rate	(bbl/d)
r_s	spherical radius	(ft)
r_w	wellbore radius	(ft)
s	skin	
t	time	(hour)

Nomenclature (continued)

Variable	Description	(Units)
T	dimensionless time integration variable	
t_D	dimensionless time	
t_{D1}	dimensionless time 1	
t_{Di}	dimensionless time i	
t_{Dk}	dimensionless time k	
t_{DL}	dimensionless linear time	
t_{Ds}	dimensionless spherical time	
v	velocity	(ft/s)
Δ	difference operator	
μ	viscosity	(cp)
ρ	density	(lbm/ft^3)
τ	dimensionless time integration variable	
ϕ	porosity	

Chapter 1.

Introduction

Oil and gas well operators use transient well testing to determine a variety of formation properties and wellbore condition. The two most commonly used pressure transient tests are the drawdown test and the buildup test. Both require constant rates during the test. A drawdown test is conducted by producing a well in a previously stabilized reservoir at a constant rate. This draws down the pressure at the sandface of the well. The bottom hole pressure recorded during the test is analyzed to provide estimates of reservoir properties. A buildup test, however, is conducted by producing a well at constant rate and then shutting the well in [1]. This allows the pressure at the sandface of the well to build up. The measured bottom hole pressure from this test can also be analyzed for reservoir properties. Buildup tests are analyzed more often than drawdown tests because a constant rate of zero is easy to maintain while a well is shut in. On the other hand, "in drawdown testing, the rate fluctuates with time, as a truly constant production rate can rarely be maintained under the field conditions" [11].

Analysts can obtain the same information about reservoir permeability and skin from either a constant rate drawdown or a buildup test. Lee [1] asserts that even reservoir pressure can be determined from a two rate drawdown test. However, drawdown tests with arbitrary flow rate variations can not be analyzed by conventional methods.

Several factors contribute to changes in production rate. Wellbore storage causes the sandface flow rate to vary during the early stage of a well test. Tubing liquid loading or hydrates in the tubing cause temporary flow interruptions. Surface equipment malfunctions (eg. instrument failure or compressor break-down) may cause reduced flow. Gas processing plant upsets can restrict or limit gas flow. Flow is also restricted or interrupted because of natural gas market demand fluctuations.

Drawdown testing has a definite economical advantage. If drawdown tests could be analyzed in spite of the arbitrary flow rate variations, well operators could receive cash flow from production while testing. This is particularly attractive for low permeability reservoirs. In fact, some tight reservoirs exhibit such low permeability that a buildup test would not reach pseudosteady-state for years. Obviously, well owners can not tolerate such a large loss of cash flow. Thus an extended drawdown test is preferable for the purpose of obtaining reservoir parameters.

The pressure influence function of a well is defined as the dimensionless bottom hole pressure variation over time under conditions of constant sandface flow rate from the formation to the wellbore. It is affected by both the reservoir and wellbore characteristics. From a pressure influence function an analyst may identify the type of flow in the reservoir (ie. radial, linear or spherical) and estimate reservoir parameters (ie. permeability and skin).

For short flow durations, the flow rate at the tubing head of a well is rarely identical to the sandface flow rate because of the storage volume of the wellbore. Sandface flow rate can be measured and used to eliminate the masking effect of wellbore storage on the pressure influence function. This unmasking is called deconvolution.

Most existing methods of analyzing a varying rate drawdown test assume radial flow of fluids in a homogeneous reservoir. However, the reservoir may exhibit linear or spherical flow or may be of a heterogeneous nature. The use of an incorrect flow model for a given reservoir could result in erroneous permeability and skin estimates [11].

Section 1.1 Thesis Scope

In this thesis, a numerical method of deconvolving variable rate drawdown tests is proposed. Based on measured sandface flow rate and bottom hole pressure data, the method generates an ersatz constant rate pressure influence function. This pressure influence function can then be analyzed using conventional theory. The proposed method is verified using synthetic well test data and examples from the literature.

The proposed deconvolution method was tested against a greater variety of flow rate schedules than other methods reported in the literature. The flow rate schedules include multiple constant rates, linearly increasing rates, wellbore storage induced flow rate fluctuations and periodically changing flow rates. Three types of reservoir flow are considered, namely radial, linear and spherical flow.

This thesis does not consider the actual techniques of measuring sandface flow rate. Information regarding these techniques can be obtained from service companies that specialize in measuring sandface flow rate through the use of spinner surveys. This thesis assumes the availability of accurate sandface flow rate data.

Chapter 2.

Deconvolution Background

A fundamental assumption in the development of conventional well test theory is constant sandface flow rates. Any flow rate variation during a well test violates this assumption and renders the well test uninterpretable. The objective of deconvolution is to eliminate the affect of rate variation thus allowing the use of conventional well test theory.

Strictly speaking, deconvolution is a mathematical solution of the convolution integral. The convolution integral (equation 2.1) describes the bottom hole pressure response (p_{wDRef}) during a well test in which the flow rate varies. The integrand of the convolution integral contains two terms: dimensionless flow rate (q_D), and the pressure influence function (p_D). The solution of the integral for one of the integrand terms is called deconvolution. During a well test, p_{wDRef} and q_D are measured. Therefore deconvolution is used to solve equation 2.1 for p_D. This process is trivial in the case where q_D is constant, but very challenging when the flow rate varies.

Convolution Integral

$$p_{wDRef}(t_D) = \int_0^{t_D} q_D(\tau)\frac{dp_D(t_D-\tau)}{d\tau}d\tau \qquad 2.1$$

Deconvolution produces a pressure influence function (p_D) which can be used to identify the type of flow through the porous media of the reservoir. The fluid may flow radially, linearly or spherically to the wellbore. The reservoir flow model determines the type of equations required to analyze the well test data.

Equation 2.1 is known to be a Volterra equation of the first kind. The solution of this type of equation is often accomplished by use of the Laplace transforms and depends on the form of the forcing function q_D. In this thesis a method of deconvolution is proposed that is applicable to any form of q_D.

Section 2.1 Methods of Deconvolution in the Literature

Many researchers in the petroleum industry have suggested methods of deconvolving variable rate drawdown and buildup tests. In this section the deconvolution algorithms of various authors are examined.

2.1.1 Superposition

The principle of superposition is used in well testing to predict the pressure response in a reservoir as a result of varying flow rates. Superposition mathematically combines a pressure influence function and a flow rate schedule to produce the bottom hole pressure response.

Jargon and Van Poollen [2] suggest using superposition to solve variable rate well test problems. However their approach assumes radial flow. If the reservoir flow pattern for a particular well test is not radial, the reservoir parameters calculated by their method will be erroneous. Similar methods are available for linear or spherical flow regimes as well, but they too assume a single flow regime throughout the test.

2.1.2 Rate Normalization

Gladfelter, Tracy and Wilsey [3] suggested normalizing the bottom hole pressure during after-flow of a buildup test to eliminate the effect of wellbore storage. They normalized the dimensionless bottom hole pressure using

$$p_{wDRef} = p_{wD}\left(\frac{q_{Ref}}{q_{Ref} - q}\right) \qquad 2.2$$

Winestock and Colpitts [4] later suggested using this type of normalization for gas well deliverability tests with smoothly varying flow rates. They showed that for a flow rate expressed as a polynomial function of time [4],

$$\frac{p_{wD}}{q}(t) = p_D + additional \quad terms \qquad 2.3$$

in which they assert that the additional terms are negligible. This method was recommended by Lee [1] when the variations of $q(t)$ are small.

More recently a study by Kuchuk has shown that this type of deconvolution "is valid only if the down-hole flow rate varies linearly with time" [5].

2.1.3 Odeh and Jones' Variable Rate Analysis

For the conditions of radial flow, Odeh and Jones [14] proposed a method of analyzing variable rate drawdown tests by approximating the flow rate schedule with a series of discrete rate steps. Using the method of superposition for a drawdown test with n consecutive constant flow rates, they derived the equation

$$\frac{p_i - p_{wf}}{q_n} = 162.6\frac{\mu B}{kh}\left[\sum_{j=1}^{n}\frac{(q_j - q_{j-1})}{q_n}\log(t_n - t_{(j-1)})\right] + 162.6\frac{\mu B}{kh}\left[\log\left(\frac{k}{\phi\mu c_t r_w^2}\right) - 3.23 + 0.869s\right] \qquad 2.4$$

which suggests that plotting

$$\frac{p_i - p_{wf}}{q_n} \quad \text{versus} \quad \frac{1}{q_n}\sum_{j=1}^{n}(q_j - q_{j-1})\log(t_n - t_{(j-1)})$$

would produce a straight line with a slope m:

$$m = 162.6\frac{\mu B}{kh} \qquad 2.5$$

The limitations of this method include the assumption of radial flow and an infinitely large reservoir. The method also ignores wellbore storage effects during the rate changes [1].

2.1.4 Deconvolution Using Laplace Transforms

As early as 1949, van Everdingen and Hurst [6] suggested the use of the Laplace transform for convolution and deconvolution. They mathematically modelled the sandface flow rate caused by wellbore storage using a function which increases exponentially to a constant rate. Applying the Laplace transform to this model, they were able to solve the convolution integral for the constant bottom hole pressure case and the constant tubing head flow rate case.

Kucuk and Ayestaran [7] reviewed the use of Laplace transforms specifically for deconvolution. They showed that the pressure influence function can be calculated from

$$p_D(t_D) = \int_0^{t_D} K(\tau)\, p_{wD}(t_D - \tau)\, d\tau \qquad 2.6$$

where K is an inverse Laplace transform related to the dimensionless flow rate as shown below.

$$K(t_D) = \mathcal{L}^{-1}\left[\frac{1}{s\bar{q}_D(s)}\right] \qquad 2.7$$

2.1.5 Numerical Deconvolution

In an attempt to deal with well test data convolved by arbitrary flow schedules, some authors have turned to numerical methods of deconvolution. In these methods, the solution at each time point becomes a function of the solutions at all previous time points. Hamming [9] noted that most of these methods of numerical deconvolution suffer from stability problems in the form of geometrically increasing oscillation.

2.1.6 Meunier Method

In 1985, Meunier, Wittmann, and Stewart [8] proposed a numerical method of finding reservoir parameters from a buildup test with after-flow. Their method assumed radial flow and should not be used for other flow patterns.

2.1.7 Hamming Deconvolution

Hamming [9] designed a numerical deconvolution method for use in a creep and relaxation problem. He noted that the method works well for pressure influence functions that decrease with time. The method becomes unstable when p_D increases making the method unsuitable for well testing since radial, linear and spherical pressure influence functions all increase with time.

2.1.8 Deconvolution by Assuming Pressure Response

Kucük and Ayestaran [7] suggested assuming a reservoir flow pattern and curve-fitting the pressure influence function with a power series or some other function.

2.1.9 Deconvolution with Constraints

Since numerical deconvolution methods are highly susceptible to data errors, Kucuk, Carter, and Ayestaran [10] proposed a method of deconvolution that constrains the pressure influence function (p_D). They suggested the following constraints for $t \geq 0$

$$p_D \geq 0 \qquad 2.8$$

$$p'_D \geq 0$$

$$p''_D \leq 0$$

p''_D is monotonically increasing.

where p' is the derivative of pressure with respect to time.

In addition, it is required that the pressure solution be a piecewise quadratic function. They solved the convolution integral by using finite elements and a least square methods. They found that their deconvolution method was successful when flow rate noise did not exceed 2.0%.

In this thesis, another method of deconvolution is proposed that can successfully deconvolve all flow variations and flow patterns.

Chapter 3.

Proposed Deconvolution Method

The object of this thesis is to propose a deconvolution method that can be used for any arbitrary flow rate schedule. Real and significant fluctuations in flow rate are not ignored. It is not practical to represent real flow rate data as a smooth function as other researchers have done because gas and oil well production rates rarely behave smoothly. To be useful, the method of deconvolution must be able to handle flow rate schedules that include discontinuities, nonlinearities and periodic fluctuations.

Section 3.1 Method Derivation

This section outlines a novel approach to finding an unknown pressure influence function from sandface flow rate and bottom hole pressure data.

As discussed in Appendix A, the solution of the diffusivity equation for a constant rate can be expressed in general terms as

$$p_{wDRef}(t_D) = q_D p_D(t_D) \qquad 3.1$$

in which p_{wDRef} is the dimensionless bottom hole pressure function at a reference sandface flow rate (q_{Ref}). p_{wDRef} is defined by

$$p_{wDRef} = \frac{(p_i - p_{wf})kh}{141.2\mu q_{Ref}} \qquad 3.2$$

The variable q_D represents the dimensionless sandface flow rate specified by

$$q_D(t_D) = \frac{q_{sf}(t_D)}{q_{Ref}} \qquad 3.3$$

in which q_{sf} is the sandface flow rate. The symbol p_D represents the pressure influence function.

The solution in equation 3.1 assumes a constant flow rate of slightly compressible fluid and is applicable to any reservoir flow pattern. The solution can be modified for a varying flow rate using the law of superposition:

$$p_{wDRef}(t_{Dk}) = \sum_{i=0}^{k-1} [q_D(t_{Di+1}) - q_D(t_{Di})] p_D(t_{Dk} - t_{Di}) \qquad 3.4$$

where i and k are time data point counters. The notation of equation 3.4 is simplified by assuming equal time intervals and therefore letting the integers i and k replace dimensionless time t_{Di} and t_{Dk} yielding

$$p_{wDRef}(k) = \sum_{i=0}^{k-1} [q_D(i+1) - q_D(i)] p_D(k-i) \qquad 3.5$$

The forward difference Δp_{wDRef} is defined by

$$\Delta p_{wDRef}(k) = p_{wDRef}(k+1) - p_{wDRef}(k) \qquad 3.6$$

Substituting the expression for p_{wDRef} from equation 3.5 into equation 3.6 generates the following equation:

$$\Delta p_{wDRef}(k) = \sum_{i=0}^{k}[q_D(i+1) - q_D(i)]p_D(k+1-i) - \sum_{i=0}^{k-1}[q_D(i+1) - q_D(i)]p_D(k-i) \qquad 3.7$$

which may be expanded to

$$\begin{aligned}\Delta p_{wDRef}(k) = \; & [q_D(1) - q_D(0)]p_D(k+1) \\ & +[q_D(2) - q_D(1)]p_D(k) \\ & +[q_D(3) - q_D(2)]p_D(k-1) + \ldots \\ & +[q_D(k-1) - q_D(k-2)]p_D(3) \\ & +[q_D(k) - q_D(k-1)]p_D(2) \\ & +[q_D(k+1) - q_D(k)]p_D(1) \\ & -[q_D(1) - q_D(0)]p_D(k) \\ & -[q_D(2) - q_D(1)]p_D(k-1) \\ & -[q_D(3) - q_D(2)]p_D(k-2) - \ldots \\ & -[q_D(k-1) - q_D(k-2)]p_D(2) \\ & -[q_D(k) - q_D(k-1)]p_D(1)\end{aligned} \qquad 3.8$$

By collecting like terms, and stipulating that $p_D(0)=0$, equation 3.8 may be rearranged into the following form

$$\begin{aligned}\Delta p_{wDRef}(k) = \; & [q_D(1)-q_D(0)][p_D(k+1)-p_D(k)] \\ & +[q_D(2)-q_D(1)][p_D(k)-p_D(k-1)] \\ & +[q_D(3)-q_D(2)][p_D(k-1)-p_D(k-2)]+\ldots \\ & +[q_D(k-1)-q_D(k-2)][p_D(3)-p_D(2)] \\ & +[q_D(k)-q_D(k-1)][p_D(2)-p_D(1)] \\ & +[q_D(k+1)-q_D(k)][p_D(1)-p_D(0)]\end{aligned} \qquad 3.9$$

This equation may be simplified using forward difference notation

$$\begin{aligned}\Delta p_{wDRef}(k) = \; & \Delta q_D(0)\Delta p_D(k) \\ & +\Delta q_D(1)\Delta p_D(k-1) \\ & +\Delta q_D(2)\Delta p_D(k-2)+\ldots \\ & +\Delta q_D(k-2)\Delta p_D(2) \\ & +\Delta q_D(k-1)\Delta p_D(1) \\ & +\Delta q_D(k)\Delta p_D(0)\end{aligned} \qquad 3.10$$

and further simplified using summation notation

$$\Delta p_{wDRef}(k) = \Delta q_D(0)\Delta p_D(k) + \sum_{i=0}^{k-1} \Delta q_D(k-i)\Delta p_D(i) \qquad 3.11$$

Equation 3.11 may be solved for $\Delta p_D(k)$ by rearranging

$$\Delta p_D(k) = \frac{\Delta p_{wDRef}(k)}{\Delta q_D(0)} - \frac{1}{\Delta q_D(0)} \sum_{i=0}^{k-1} \Delta q_D(k-i) \Delta p_D(i) \qquad 3.12$$

Replacing the integer k with t_{Dk}, equation 3.12 can be restated in terms of dimensionless time as

$$\Delta p_D(t_{Dk}) = \frac{\Delta p_{wDRef}(t_{Dk})}{\Delta q_D(0)} - \frac{1}{\Delta q_D(0)} \sum_{i=0}^{k-1} \Delta q_D(t_{Dk} - t_{Di}) \Delta p_D(t_{Di}) \qquad 3.13$$

Equation 3.13 expresses the solution for the forward difference of the pressure influence function at time t_{Dk} in terms of all of the previously computed values of this function. The pressure influence function may be calculated by summation of the forward difference function [9].

$$p_D(k) = \sum_{i=0}^{k-1} \Delta p_D(i) \qquad 3.14$$

Equation 3.13 and 3.14 represent a new method of deconvolving variable rate well test data to obtain the constant rate pressure influence function of the well. The method requires knowledge of p_{wDRef} (obtained from bottom hole pressure data) and sandface flow rate. The derivation has not restricted the type of reservoir flow pattern nor the type of flow rate schedule. The method uses discrete summation and difference techniques applicable to data points sampled at equal time intervals and assumes that $p_D(0)=0$.

Section 3.2 Practical Concerns

Three practical concerns are associated with equation 3.13. Firstly, bottom hole pressure data are rarely measured at equal time intervals. Secondly, the division of the right hand side of equation 3.13 by $\Delta q_D(0)$ could cause round off error. Lastly, when interpreting a well test, the reservoir parameters required to calculate the dimensionless bottom hole pressure (p_{wDRef}) are unknown.

The fact that equation 3.13 requires data at equally spaced time intervals is not a serious drawback. Several techniques including linear interpolation may be used to interpolate such data points from the raw data.

The denominator of the right hand side of Equation 3.13 is $\Delta q_D(0)$, the difference between the dimensionless flow rate at time 1 and at time 0. The difference is defined as

$$\Delta q_D(0)=\frac{q(1)}{q_{ref}}-\frac{q(0)}{q_{ref}} \qquad 3.15$$

To reduce the round off error in equation 3.13, q_{ref} should be set to the value of the first flow rate data point:

$$q_{ref}=q(1) \qquad 3.16$$

This, in addition to the fact that the well is not initially flowing, reduces equation 3.15 to

$$\Delta q_D(0) = \frac{q(1)}{q(1)} - \frac{0}{q(1)} = 1 \qquad 3.17$$

and simplifies equation 3.13 to

$$\Delta p_D(t_{Dk}) = \Delta p_{wDRef}(t_{Dk}) - \sum_{i=0}^{k-1} \Delta q_D(t_{Dk} - t_{Di}) \Delta p_D(t_{Di}) \qquad 3.18$$

eliminating a potential source of round off error.

Equation 3.13 requires the calculation of the dimensionless bottom hole pressure p_{wDRef} as defined by equation 3.2. However, when interpreting a well test, the analyst rarely knows the permeability k of the formation needed in equation 3.2. Indeed, one major purpose of well testing is to deduce this parameter.

To work with bottom hole pressure directly rather than p_{wDRef}, equation 3.2 is expressed as

$$p_{wDRef}(t) = \frac{p_i - p_{wf}(t)}{m} \qquad 3.19$$

in which m is a constant related to parameters of the reservoir. If the bottom hole pressure difference p_{wd} is defined by

$$p_{wd}(t) = p_i - p_{wf}(t) \qquad 3.20$$

then equation 3.19 can be expressed as

$$p_{wDRef}(t) = \frac{p_{wd}(t)}{m} \tag{3.21}$$

Equation 3.21 is substituted into equation 3.13 to produce

$$\Delta p_D(t_k) = \frac{\Delta p_{wd}(t_k)}{m\Delta q_D(0)} - \frac{1}{\Delta q_D(0)}\sum_{i=0}^{k-1}\Delta q_D(t_k - t_i)\Delta p_D(t_i) \tag{3.22}$$

Multiplying Equations 3.22 and 3.14 by m yields

$$m\Delta p_D(t_k) = \frac{\Delta p_{wd}(t_k)}{\Delta q_D(0)} - \frac{1}{\Delta q_D(0)}\sum_{i=0}^{k-1}\Delta q_D(t_k - t_i)m\Delta p_D(t_i) \tag{3.23}$$

and

$$m p_D(k) = \sum_{i=0}^{k-1} m\Delta p_D(i) \tag{3.24}$$

In a constant rate well test, the bottom hole pressure and pressure influence function are related by

$$p_i - p_{wf} = m p_D \tag{3.25}$$

This relationship also applies to a deconvolved well test if the bottom hole pressure is replaced with the deconvolved bottom hole pressure, $\hat{p}_{wf}$.

$$p_i - \hat{p}_{wf} = m p_D \tag{3.26}$$

Therefore the pressure influence function is also related to the deconvolved bottom hole pressure difference by

$$\hat{p}_{wd} \equiv p_i - \hat{p}_{wf} = m p_D \tag{3.27}$$

Thus equation 3.24 calculates the deconvolved bottom hole pressure difference $\hat{p}_{wd}(t)$. Modifying equations 3.23 and 3.24 with this information yields

$$\Delta\hat{p}_{wd}(t_k)=\frac{\Delta p_{wd}(t_k)}{\Delta q_D(0)}-\frac{1}{\Delta q_D(0)}\sum_{i=0}^{k-1}\Delta q_D(t_k-t_i)\Delta\hat{p}_{wd}(t_i) \qquad 3.28$$

and

$$\hat{p}_{wd}(k)=\sum_{i=0}^{k-1}\Delta\hat{p}_{wd}(i) \qquad 3.29$$

Therefore, if p_{wd} is used in place of p_{wDRef} in equation 3.13, then the deconvolution method calculates $\hat{p}_{wd}$ instead of p_D. In this way, the proposed method can be used to deconvolve bottom hole pressure data directly.

Section 3.3 Well Test Analysis Using the Proposed Deconvolution Method

The analysis of a variable rate drawdown test becomes as simple as analyzing a constant rate drawdown test after using the proposed deconvolution method. The following outline details the steps involved in analyzing a drawdown test using the proposed deconvolution method.

1. Interpolate bottom hole pressure data and sandface flow rate data at equally spaced time intervals. The proposed deconvolution method requires evenly spaced bottom hole

pressure and sandface flow rate data, but field data are rarely measured at equal time intervals. Data may be interpolated using linear interpolation, or cubic splines.

2. Deconvolve the bottom hole pressure using the sandface flow rate data and the proposed method. Use equations 3.28 and 3.29 as shown in the algorithm in Figure 3-1. After the bottom hole pressure is deconvolved, calculate the derivative of the data using any of the numerical differentiation algorithms proposed in the literature [15].

3. Identify the reservoir model(s) in the test. Plot $\hat{p}_{wd}$ and its derivative against time on log-log coordinates in order to identify the segments of the test affected by different reservoir flow models. Choose a conventional or type curve analysis method for each separate flow model segment identified.

4. Analyze each segment of the deconvolved data to find the reservoir parameters. The deconvolved variables $\hat{p}_{wf}$ and $\hat{p}_{wd}$ can be used in the analysis methods chosen in step 3 above as if the well was tested at a constant rate. For example, for a segment of a well test that exhibits infinite radial flow, one might analyze it using the log-log plot created in step 3 in conjunction with type curve analysis, or by creating a semi-log plot of pressure $\hat{p}_{wf}$ versus the log of time.

Deconvolution Algorithm

PURPOSE: To deconvolve the bottom hole pressure of a drawdown test given the sandface flow rate.

INPUT: number of data points $N+1$; initial reservoir pressure p_i; sandface flow rate data points $q_{sf}(k)$ and bottom hole pressure data points $p_{wf}(k)$ at equal time intervals where $0 \le k \le N$.

OUTPUT: deconvolved bottom hole pressure $\hat{p}_{wf}(k)$ where $0 \le k \le N-1$.

Step 1 Set $q_{ref} = q_{sf}(1)$.

Step 2 Set $p_{wd}(1) = p_i - p_{wf}(1)$.

Step 3 For $k = 1, \ldots, N$ do Steps 4-7.

Step 4 Let $q_D(k) = q_{sf}(k)/q_{ref}$

Step 5 Let $\Delta q_D(k-1) = q_D(k) - q_D(k-1)$

Step 6 Let $p_{wd}(k) = p_i - p_{wf}(k)$

Step 7 Let $\Delta p_{wd}(k-1) = p_{wd}(k) - p_{wd}(k-1)$

Step 8 Let $\Delta \hat{p}_{wd}(0) = \Delta p_{wd}(0)/\Delta q_D(0)$

Step 9 Let $\hat{p}_{wd}(0) = 0$

Step 10 For $k = 1, \ldots, N$ do Steps 11-15.

Step 11 Let $\Delta \hat{p}_{wd}(k) = \Delta p_{wd}(k)$.

Step 12 For $i = 0, \ldots, k-1$

Let $\Delta \hat{p}_{wd}(k) = \Delta \hat{p}_{wd}(k) - \Delta \hat{p}_{wd}(i) \Delta q_D(k-i)$.

Step 13 Let $\Delta \hat{p}_{wd}(k) = \Delta \hat{p}_{wd}(k)/\Delta q_D(0)$.

Step 14 Let $\hat{p}_{wd}(k) = \hat{p}_{wd}(k-1) + \Delta \hat{p}_{wd}(k-1)$.

Step 15 Set $\hat{p}_{wf}(k) = p_i - \hat{p}_{wd}(k)$.

Figure 3-1 Proposed Deconvolution Algorithm

Chapter 4.

Testing of the Proposed Deconvolution Method

The validity and accuracy of the proposed deconvolution method were tested using simulated well test data. The nineteen well test simulations included linear, radial and spherical reservoir flow models with several varying sandface flow rate schedules. Each set of simulated bottom hole pressure data p_{wDRef} was created by convolving a pressure influence function p_D and a sandface flow rate function q_D. The bottom hole pressure data p_{wDRef} were subsequently deconvolved using the proposed method to produce a pressure influence function which was compared to the original p_D.

In addition to the nineteen synthetic well tests, two variable rate well tests reported in the literature were deconvolved and analyzed. The resulting reservoir parameters were compared with those in the original publications.

Section 4.1 Reservoir Flow Models

The proposed deconvolution method was tested with three types of reservoir flow models; radial, linear and spherical. Each type of flow assumes different orientation of flowlines within the reservoir as shown in Figure 4-1.

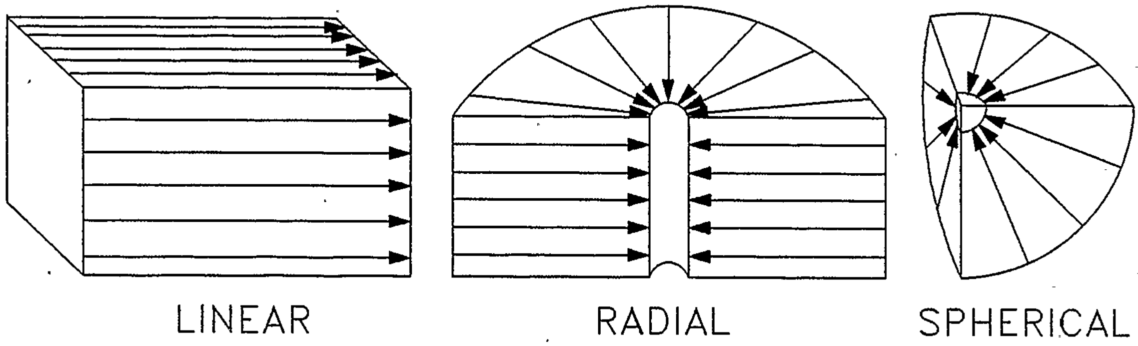

Figure 4-1. Three Reservoir Flow Models [13]

A. Radial Flow

The pressure transient behavior in a homogeneous reservoir in which radial flow occurs to a wellbore of infinitesimally small radius is described by the exponential integral solution or the log approximation of this solution [11]. The log approximation states

$$p_D = \frac{1}{2}\left[\ln\left(\frac{t_D}{r_D^2}\right) + 0.809 \right] \tag{4.1}$$

At the wellbore, r_D becomes unity and the semi-log pressure derivative of the pressure influence function is a constant 0.5 as shown in Figure 4-2.

$$p'_D = \frac{1}{2} \tag{4.2}$$

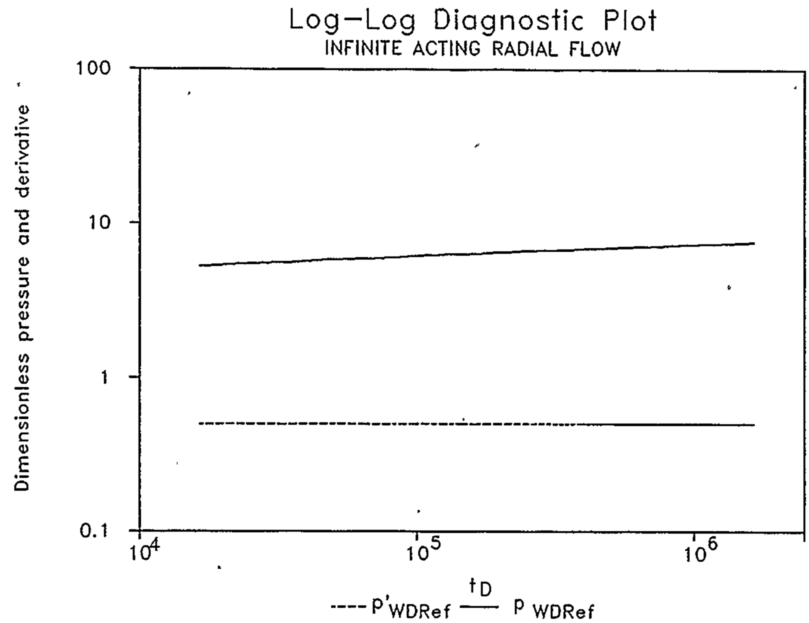

Figure 4-2. Pressure Influence Function of a Well Test Exhibiting Radial Flow in the Reservoir

Table 4.1. Reservoir Parameters Used to Model Synthetic Pressure Response in an Infinite Cylindrical Reservoir

Reservoir Parameter	Parameter Value	Units
k	12.	mD
h	10.	ft
μ	1.2	cp
r_w	0.40	ft
ϕ	10.%	
c_t	1.0e-5	1/psi
p_i	3000.	psia
q_{ref}	100.	STB/day
B_o	1.2	bbl/STB

For the synthetic well with parameters listed in Table 4.1, dimensionless time is related to real time by

$$t_D = \frac{2.637 \times 10^{-4} kt}{\phi \mu c_t r_w^2} \tag{4.3}$$

$$= \frac{2.637 \times 10^{-4}(12)t}{0.10(1.2)(1 \times 10^{-5})(0.40)^2}$$

$$= 16481.25t$$

Incorporating this result, the pressure influence function is

$$p_D = \frac{1}{2}[\ln(16481.25t) + 0.809] \tag{4.4}$$

B. <u>Linear Flow</u>

In a hydraulically fractured reservoir, fluid flows from the reservoir to the fracture in a linear flow pattern. During a constant rate well test of a reservoir with a linear flow pattern, the pressure influence function and its derivative both exhibit a slope of 1/2 on a log-log plot as shown in Figure 4-3.

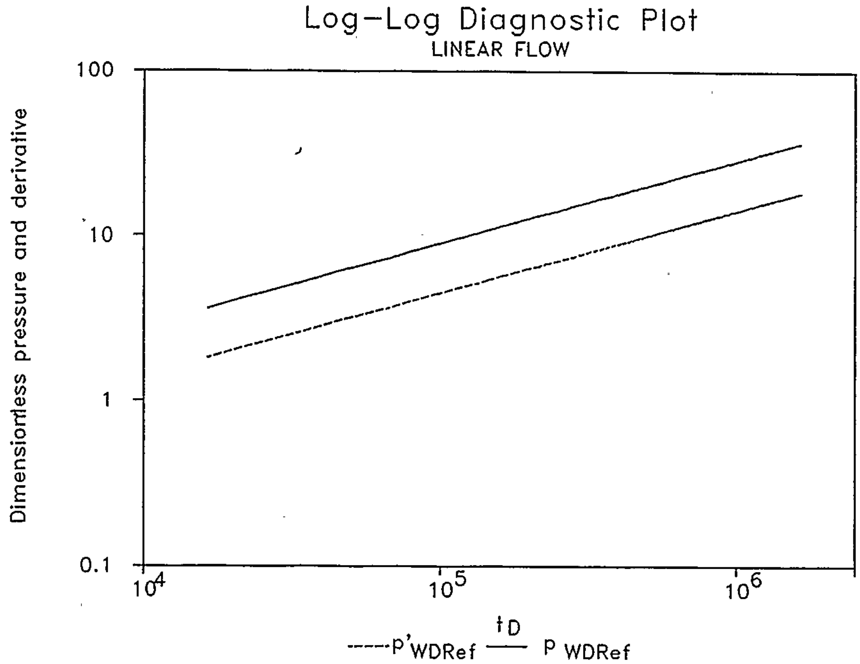

Figure 4-3. Pressure Influence Function of a Well Test Exhibiting Linear Flow in the Reservoir

Table 4.2. Reservoir Parameters Used to Model Synthetic Pressure Response in a Hydraulically Fractured Reservoir Exhibiting Linear Flow

Reservoir Parameter	**Parameter Value**	**Units**
k	12.	mD
h	10.	ft
μ	1.2	cp
r_w	0.40	ft
ϕ	10.%	
c_t	1.0e-5	1/psi
p_i	3000.	psia
q_{ref}	100.	STB/day
B_o	1.2	bbl/STB
L	50.	ft

The pressure influence function p_D for linear flow is mathematically expressed following Streltsova's solution [12] as

$$p_D = 3.5449\sqrt{t_{DL}} \qquad 4.5$$

where

$$t_{DL} = \frac{2.637\times 10^{-4} kt}{\phi \mu c_t L^2} \qquad 4.6$$

Using the reservoir parameters of Table 4.2, equation 4.6 becomes

$$t_{DL} = \frac{2.637\times 10^{-4}(12)t}{0.10(1.2)(1\times 10^{-5})(50)^2} \qquad 4.7$$

$$= 1.0548t$$

and the dimensionless bottom hole pressure is

$$p_D = 3.641\sqrt{t} \qquad 4.8$$

with a derivative of

$$p'_D = 1.821\sqrt{t} \qquad 4.9$$

C. Spherical Flow

During a constant rate well test of a reservoir with a spherical flow pattern, the pressure derivative exhibits a slope of -1/2 on a log-log plot as shown in Figure 4-4.

The pressure influence function for spherical flow at late time [11] is expressed by

$$p_D = 1 - \frac{1}{\sqrt{\pi t_{Ds}}} \qquad 4.10$$

where

$$t_{Ds} = \frac{2.637 \times 10^{-4} k_s t}{\phi \mu c_t r_s^2} \qquad 4.11$$

$$k_s = (k_r k_z^{1/2})^{2/3} \qquad 4.12$$

and

$$r_s = \left(\frac{r_w h}{2}\right)^{1/2} \left(\frac{k_z}{k_r}\right)^{1/4} \qquad 4.13$$

Using the synthetic well with parameters listed in Table 4.3, the spherical permeability and radius are

$$k_s = 55.7\,mD \qquad 4.14$$

and

$$r_s = 44.72\,ft \qquad 4.15$$

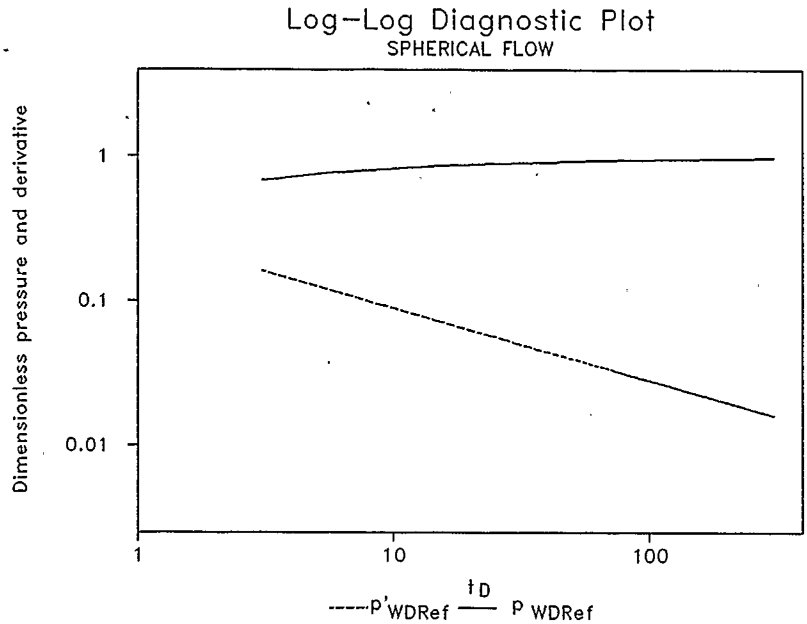

Figure 4-4. Pressure Influence Function of a Well Test Exhibiting Spherical Flow in the Reservoir

Table 4.3. Reservoir Parameters Used to Model Synthetic Pressure Response of a Reservoir Exhibiting Spherical Flow

Reservoir Parameter	**Parameter Value**	**Units**
k_r	12.	mD
k_z	1200.	mD
h	1000.	ft
μ	1.2	cp
r_w	0.40	ft
ϕ	20.%	
c_t	1.0e-5	1/psi
p_i	3000.	psia
q_{ref}	100.	STB/day
B_o	1.2	bbl/STB

Therefore the equation for dimensionless spherical time is expressed as

$$t_{Ds} = \frac{2.637 \times 10^{-4}(55.7)t}{0.20(1.2)(1 \times 10^{-5})(44.72)^2} \qquad 4.16$$

$$= 3.060t$$

and the pressure influence function for this synthetic well is

$$p_D(t_D) = 1 - \frac{1}{3.101\sqrt{t}} \qquad 4.17$$

with a derivative of

$$p'_D(t_D) = -\frac{1}{6.202\sqrt{t}} \qquad 4.18$$

D. Composite Reservoir Flow Model

To establish the validity of the proposed deconvolution method for well tests that feature several consecutive flow reservoir patterns, some of the simulations were conducted with a composite pressure influence function. For example, a well situated in a linear sand bar might exhibit radial flow initially followed by linear flow. Such a system was modelled by assuming a pressure influence function described by

$$p_D = \left\{ \begin{array}{ll} \frac{1}{2}[\ln(16481.25t) + 0.809], & t < 25 \\ 1.3738\sqrt{t}, & t \geq 25 \end{array} \right\} \qquad 4.19$$

with a derivative of

$$p'_D = \begin{Bmatrix} \frac{1}{2}, & t < 25 \\ 0.6869\sqrt{t}, & t \ge 25 \end{Bmatrix} \qquad 4.20$$

This expression for p_D implies an abrupt transition from radial flow to linear flow at 25 hours. The transition is evident in Figure 4-5.

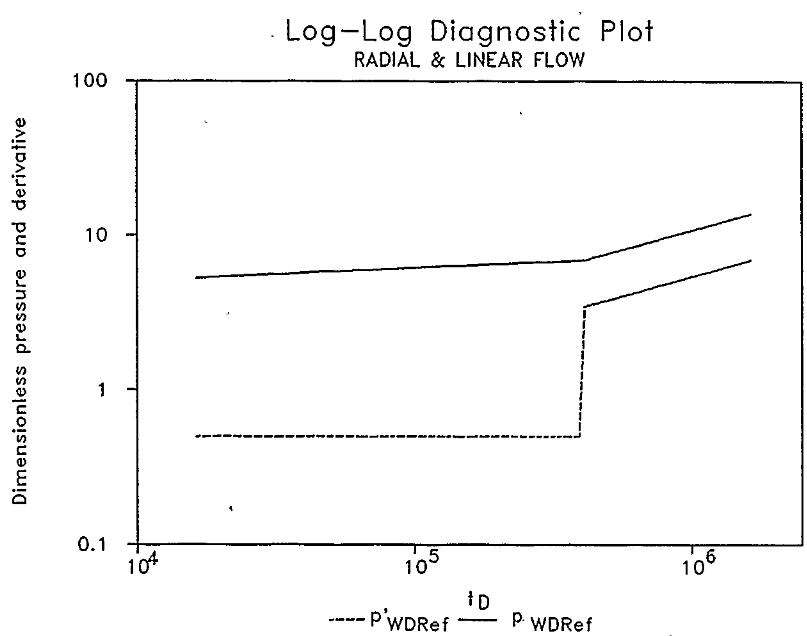

Figure 4-5. Pressure Influence Function of a Well Test Exhibiting Composite (Radial and then Linear) Flow in the Reservoir

Section 4.2 Sandface Flow Rate Schedules

Although each of the methods discussed in Chapter 2 were restricted in their treatment of flow schedules, a very reliable deconvolution method should successfully deconvolve many different schedules. The simulated bottom hole pressure data used for testing the proposed method incorporates five different types of sandface flow rate schedules including constant flow rates, linearly changing flow rates, wellbore storage affected rates, periodic rates, and multiple consecutive constant rates.

1. Constant Flow Rate

The first sandface flow rate schedule studied was the trivial case of the constant rate. Strictly speaking, this flow rate schedule needs no deconvolution at all. However, an accurate deconvolution method should apply to this model as well as more exotic flow schedules. The synthetic well test data were generated using a reference constant flow rate of 120 barrels of oil per day. The mathematical description of this flow schedule is

$$q(t)=\begin{Bmatrix} 0, & t=0 \\ 120, & t\geq 0 \end{Bmatrix} \qquad 4.21$$

2. Linearly Increasing Rate

Since some drawdown tests have sandface flow rate schedules that increase linearly through part of the test, the proposed deconvolution method has been tested with this flow schedule to assure its stability. The flow schedule used to generate synthetic well test data was chosen so as to increase the flow rate to 120 barrels of oil per day in 50 days and is described by

$$q(t) = 0.1t \tag{4.22}$$

3. Exponential Increase to a Constant Rate

The effect of wellbore storage on sandface flow rate is often simulated by an exponential increase to a constant rate [6] as shown in Figure 4-6. The proposed deconvolution method has been tested using a flow rate schedule that increased to 99.9% of 120 barrels per day in 24 hours. The wellbore storage flow rate schedule is mathematically modeled by

$$q(t) = 120(1 - e^{-0.3t}) \tag{4.23}$$

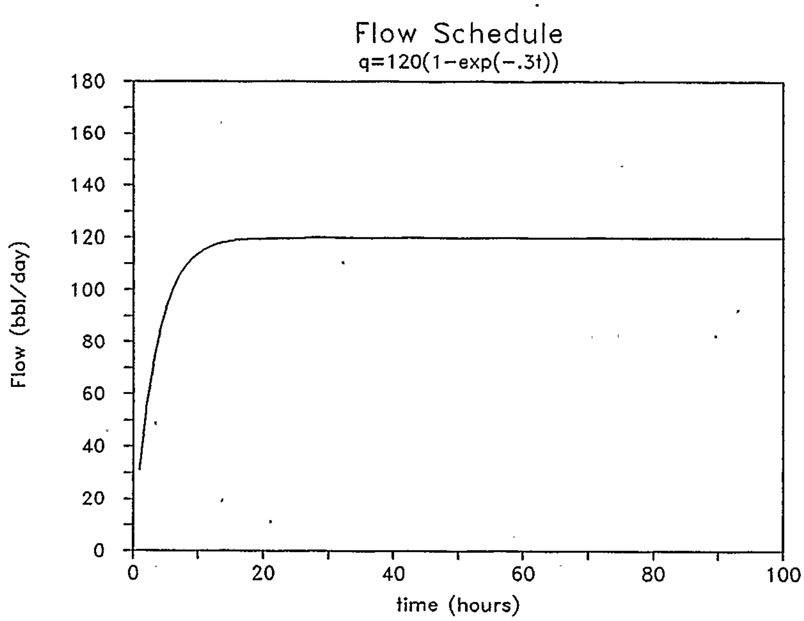

Figure 4-6. Wellbore Storage Sandface Flow Rate Schedule

4. Cosinusoidal Rate

Some flow rate schedules feature periodic fluctuation. To simulate such periodic flow a cosinusoidal flow rate schedule was studied. As shown in Figure Figure 4-7, this flow schedule was designed to have a period of about 12 hours and to stay above 120 bbl/d. It is expressed mathematically by

$$q(t) = 120[\cos(0.5t) + 2] \qquad 4.24$$

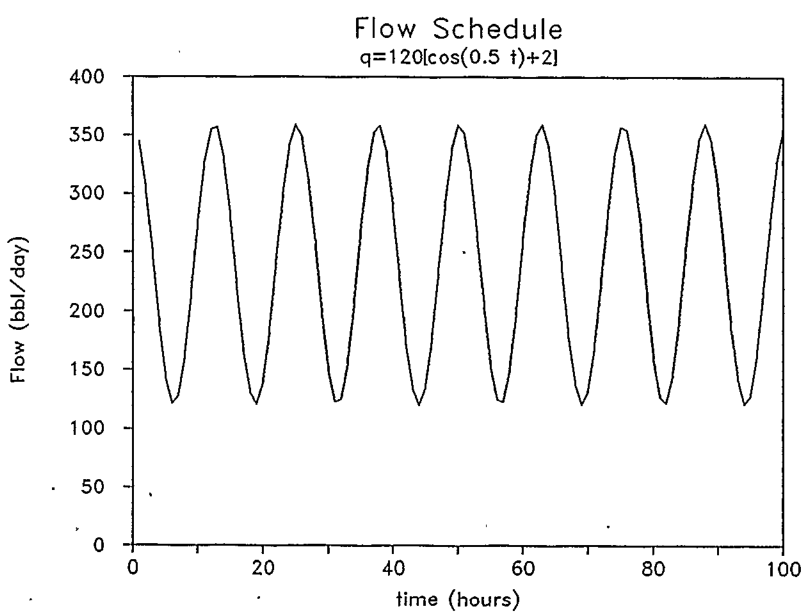

Figure 4-7. Cosine Periodic Sandface Flow Rate Schedule

5. Multiple Consecutive Constant Rates

Finally, many flow schedules can be approximated through a consecutive series of constant rates. Therefore a multiple rate flow schedule was considered to test the stability of the proposed method. The sandface flow rate followed the following form:

$$q(t)=\begin{Bmatrix} 0, & t=0 \\ 60, & 0<t<25 \\ 120, & 25=<t<50 \\ 90, & 50=<t<75 \\ 60, & 75=<t<100 \end{Bmatrix} \qquad 4.25$$

Section 4.3 Simulation Cases

Each simulated well test was generated by convolving one pressure influence function from Section 4.1 with a sandface flow rate schedule from Section 4.2. The simplest method of simulating the well test bottom hole pressure profile is to use the principle of superposition as described by equation 3.4 to discretely convolve p_D and q_D. This is the same as assuming that the sandface flow rate is not a continuous function, but a series of discrete forward difference step functions as shown in Figure 4-8. The discrete convolution method of equation 3.4 was used to simulate bottom hole pressure for seventeen of the test cases.

$$p_{wDRef}(t_{Dk})=\sum_{i=0}^{k-1}[q_D(t_{Di+1})-q_D(t_{Di})]p_D(t_{Dk}-t_{Di}) \qquad 3.4$$

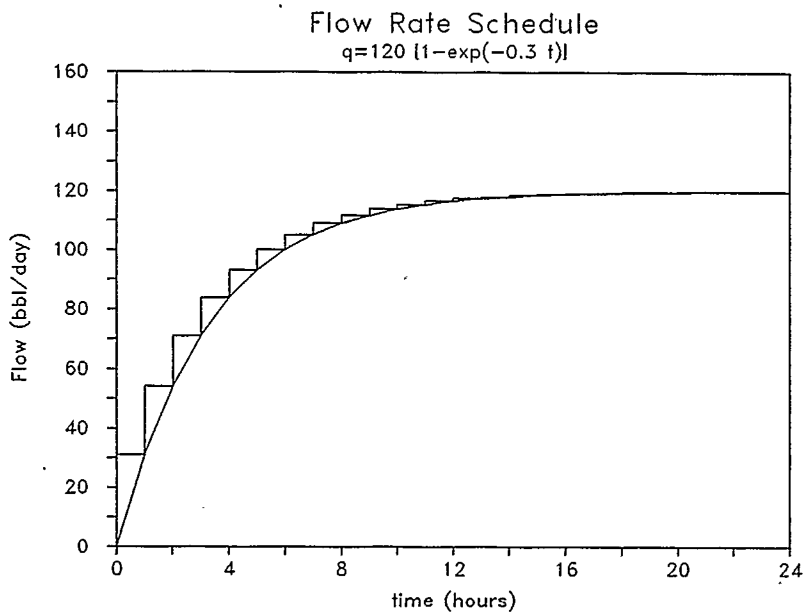

Figure 4-8. Wellbore Storage Sandface Flow Rate as a Discrete Function

A more rigorous yet difficult method of simulating well test bottom hole pressure is to continuously convolve p_D with q_D using the convolution integral (equation 2.1).

$$p_{wDRef.} = \int_0^{t_D} \frac{dq_D(\tau)}{d\tau} p_D(t_D - \tau) d\tau \qquad 2.1$$

Since the integration becomes very involved, only two of the synthetic well tests were generated in this manner. In the first of these (case A3C), the log approximation for radial flow was convolved with the wellbore storage flow schedule. The solution to the convolution integral for this simulation follows that of Streltsova's [12] and is detailed in Appendix B. Streltsova treated solutions to the convolution integral for radial flow patterns only.

The second continuously convolved simulation (case B3C) used the linear flow pressure influence function and the wellbore storage sandface flow schedule. The details of the integration involved may be found in Appendix C.

Section 4.4 Simulation Results

Simulation case numbers and descriptions are displayed in Table 4.4. All the bottom hole pressure profiles were discretely convolved using equation 3.4 except cases A3C and B3C which were continuously convolved using equation 2.1.

Table 4.4. Well Test Simulation Cases.

	Flow rate Schedules	Reservoir Flow Models A Radial	B Linear	C Spherical	D Composite
1	Constant	A1	B1	C1	-
2	Linear Increasing	A2	B2	C2	D2
3	Wellbore Storage	A3	B3	C3	-
3C	Wellbore Storage *	A3C	B3C	-	-
4	Cosinusoidal	A4	B4	C4	D4
5	Multiple Constant Rates	A5	B5	C5	-

Note: All cases were discretely convolved using equation 3.4 except as otherwise noted.
* Cases A3C and B3C were continuously convolved using equation 2.1.

The advantage of the proposed deconvolution method is apparent from Figures 4-9 through 4-12. These show that the deconvolved pressure data and derivatives compare well with the original constant rate pressure influence functions for all well test simulation cases.

Appendix D documents the well test simulations graphically. For each simulation case, the various stages of the simulation are presented; the synthetic pressure influence function, the sandface flow rate schedule, the convolved bottom hole pressure response, and the deconvolved pressure influence function.

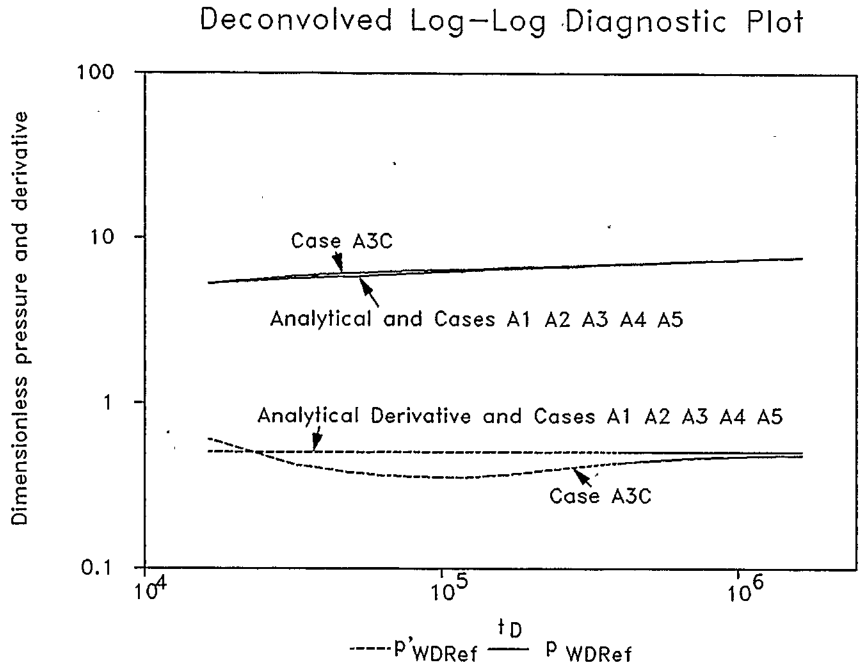

Figure 4-9. Comparison of Deconvolved Radial Flow Models

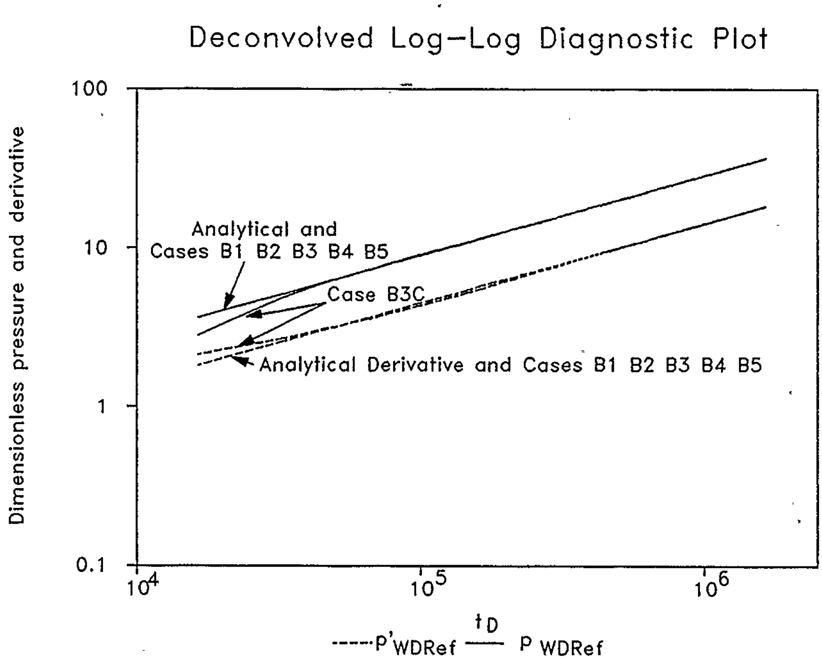

Figure 4-10. Comparison of Deconvolved Linear Flow Models

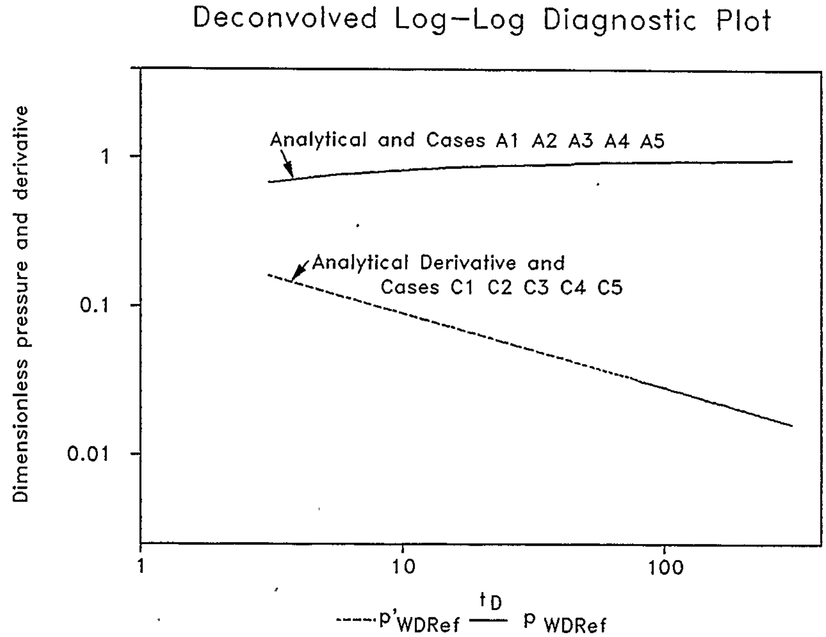

Figure 4-11. Comparison of Deconvolved Spherical Flow Models

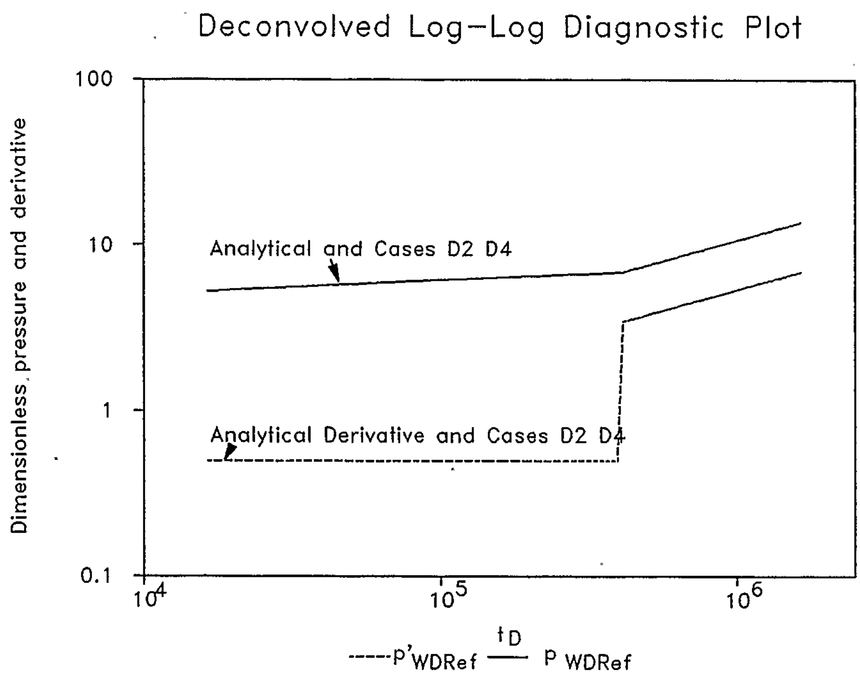

Figure 4-12. Comparison of Deconvolved Composite (Radial and then Linear) Flow Models

Section 4.5 Deconvolving Examples from Literature

In addition to the nineteen simulations summarized above, two varying rate well tests from the literature were deconvolved. The first is a well test identified by Lee [1] as Example 3.3. He used it to illustrate the rate normalization method described in this thesis in Section 2.1.2 on page 7. Appendix E contains the deconvolution and analysis details of this well test, using the proposed deconvolution method.

Figures 4-13 and 4-14 were used to analyze the deconvolved pressure response. As reported in Appendix E, the permeability and skin compare closely with those calculated by Lee using the rate normalization method (see Table 4.5).

Table 4.5 Lee's Varying Rate Well Test Example. Reservoir Parameters Calculated in Reference 1 and This Work

Reservoir Parameter	This Work	Reference 1	Difference
Permeability (mD)	7.2	7.4	-0.2
Skin	5.5	6.0	-0.5

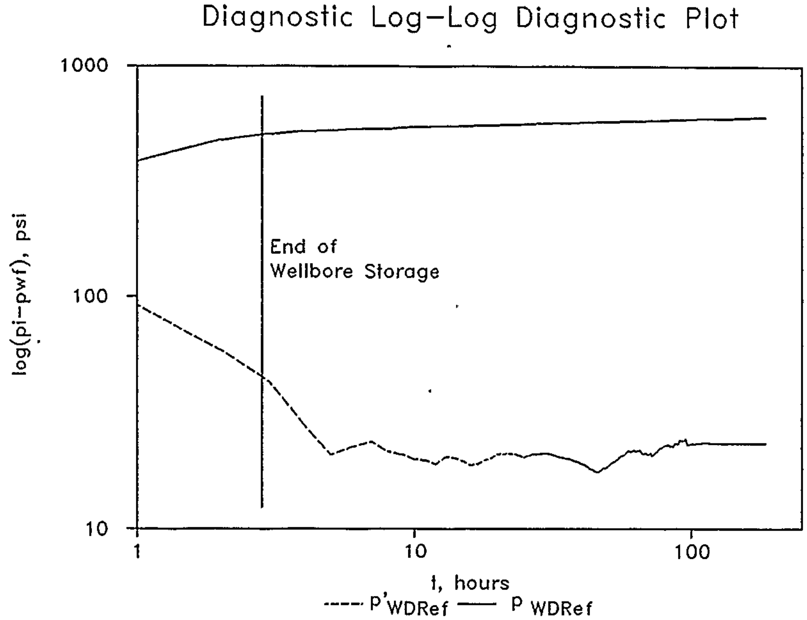

Figure 4-13. Pressure Response of Lee's Varying Rate Well Test Example After Deconvolution

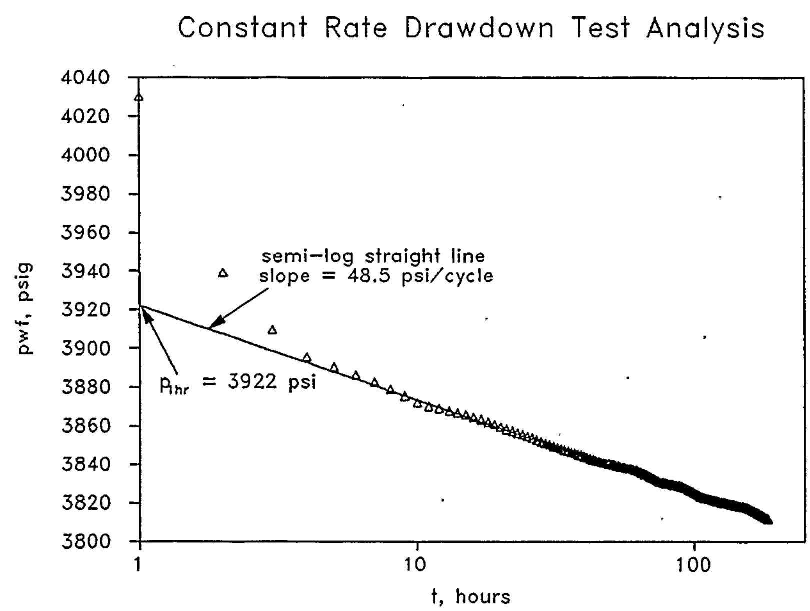

Figure 4-14. Analysis of Lee's Varying Rate Well Test Example After Deconvolution

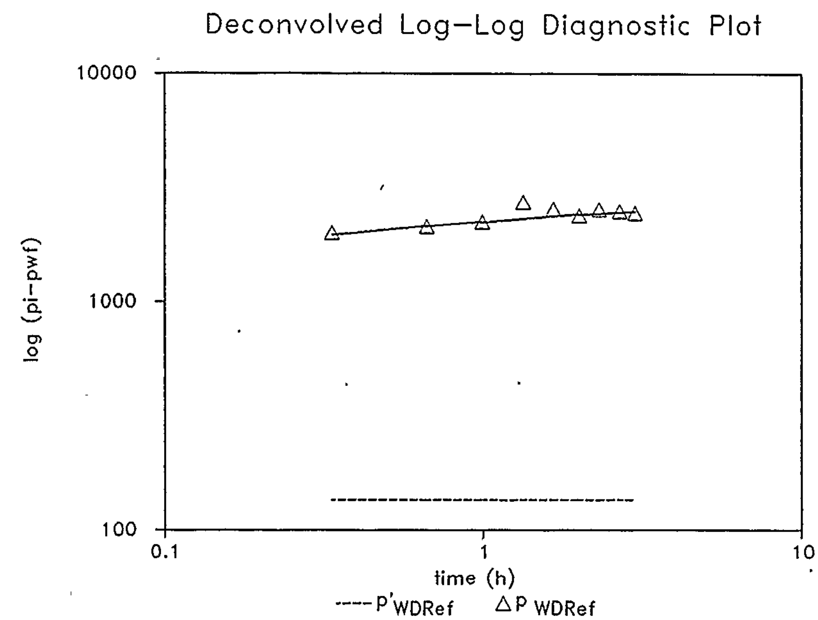

Figure 4-15. Pressure Response of Odeh and Jones' Three Rate Well Test Example After Deconvolution

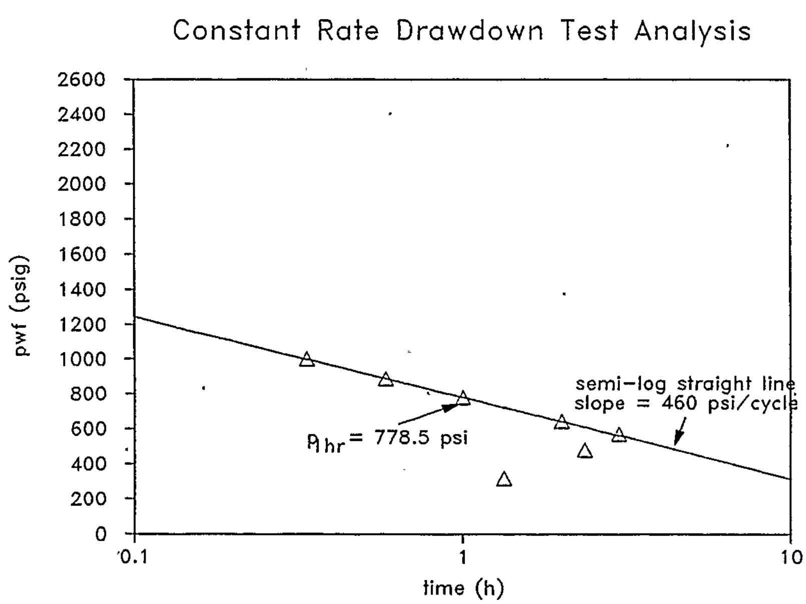

Figure 4-16. Analysis of Odeh and Jones' Three Rate Well Test Example After Deconvolution

The proposed deconvolution method was also tested using an example presented by Odeh and Jones [14]. Their three rate well test is deconvolved and analyzed in Appendix F. Figures 4-15 and 4-16 show how the deconvolved data were used to analyze the well test. As shown in Table 4.6, the reservoir parameters calculated by the proposed method agree closely with those published in the literature [1,14]. Because Odeh and Jones did not publish a skin value, the published skin in Table 4.6 is from Lee [1].

Table 4.6 Odeh and Jones' Three Rate Well Test Example. Reservoir Parameters as Calculated in the Literature and This Work

Reservoir Parameter	This Work	Published Values	Difference
Permeability-height (mD-ft)	102	103	-1
Skin	0.43	0.53	-0.1

Chapter 5.

Discussion of Results

The results presented in the previous chapter show that the proposed deconvolution method is very successful. For each synthetic well test, the deconvolved pressure response was so similar to the original pressure influence function that the same well test type curve matches both. In addition, the proposed method produced reservoir parameters very similar to those published for the two well tests taken from the literature. In this chapter the results of the various tests are discussed and the potential benefits of the method are explored.

Section 5.1 Synthetic Well Tests

The deconvolved pressure responses for all the synthetic well test cases generated by the discrete equation 3.4 compared identically to their original pressure influence functions (see Figures 4-9 through 4-12). This is to be expected since the proposed deconvolution method was also developed using equation 3.4.

It can be seen in Figures 4-9 and 4-10 that the continuously convolved simulations (cases A3C and B3C) vary slightly from the original pressure influence function. The variation is greatest at early times. This variation is due to the fact that the bottom hole pressure was simulated using continuous convolution as suggested by equation 2.1, but was deconvolved using the proposed method which is based on evenly spaced discrete equation 3.4. The deconvolved response matches the original pressure influence function best at late times when there is little change between evenly spaced data points. Even so, the deconvolved pressure and the original pressure influence function of cases A3C and B3C are so similar that they are matched by the same type curve. In well tests where early time variation becomes significant, a smaller step size could be used to reduce the variance.

These excellent results indicate that the proposed deconvolution method can handle a variety of flow rate schedules very well. The algorithm is very stable when faced with discontinuous or periodic flow rate schedules such as the multiple flow rate schedule and the periodic cosine flow schedule.

The results also indicate that the proposed method can be used regardless of the type of reservoir flow pattern affecting the well test. It performs equally well for radial, linear and spherical flow. It also handles flow pattern changes during well tests.

Section 5.2 Literature Examples

The deconvolved results of the two examples taken from Lee [1], and Odeh and Jones [14] show that the proposed deconvolution method can be used for many different types of flow variations. Lee and Odeh both suggested different methods to analyze their variable rate well test, however, one author's deconvolution method will not deconvolve the other's data. On the other hand, the deconvolution method proposed in this work, can deconvolve both data sets as well as many other types.

To maximize the utility of the proposed deconvolution method, it is important to obtain accurate sandface flow rate data. In Lee's varying flow rate example, the surface flow changes were recorded instead of the sandface flow rate. With this information, the proposed method was able to deconvolve changes evident in the surface flow rate, but was unable to unmask the wellbore storage affect. If the flow rate data had been measured at the sandface, even the wellbore storage period of the test would have been deconvolved.

Sandface flow rate data measurement should be frequent enough to capture all flow variations. As discussed in Appendix F, anomalies appeared in the deconvolved data because the three rate well test of Odeh and Jones had more flow rate variation than was reported. Indeed, Odeh and Jones state that the flow rates were averaged over each hour [14]. Flow rate averaging introduces error and is unnecessary when using the proposed deconvolution method. Even with the noise introduced by flow rate averaging, the deconvolved Odeh data was readily analyzed.

Section 5.3 Benefits of the Method

Use of the proposed deconvolution method will improve confidence in permeability and skin estimates calculated from well tests by increasing confidence in analysis methods and providing better data to analyze. Firstly, the method can be used to eliminate the effect of wellbore storage enabling analysis of a greater portion of well test data. In addition, the method can deconvolve tests in which arbitrary flow rate changes occur. If data deconvolved by the method is used in constructing diagnostic log-log plots, identification of the correct reservoir model can be made with more confidence. This improves confidence in selecting the correct reservoir analysis procedures.

Using the proposed deconvolution method, drawdown tests can be confidently analyzed. Reservoir engineers are often hesitant to conduct buildup tests on wells which produce high cashflow, but drawdown tests can rarely be analyzed because of the inevitable flow rate changes. The proposed method eliminates rate change concerns for any type of flow schedule and for any reservoir flow pattern. Continuous cash flow from wells on test may now be a reality.

The proposed method also creates deconvolved drawdown data from buildup tests. Use of equation 3.13 or 3.28 requires that the difference between the flow rate at time zero and the flow rate at the first time point ($\Delta q_D(0)$) be non-zero. Since buildup tests require a flow period before the shut-in period, the non-zero $\Delta q_D(0)$ requirement is satisfied. When buildup tests are deconvolved they can be used in conjunction with drawdown type curves without regard to the usual restriction that the shut-in time be less than 10% of the producing time. In the process, afterflow effects during buildup tests are also eliminated.

Practical concerns make it impossible to test many wells because of rate variations, lengthy wellbore storage affects, or lengthy time to stabilization. The proposed deconvolution method increases the scope of wells that can be tested. The proposed method can be especially useful for testing low permeability wells. Such wells require very long duration drawdown tests to investigate further than a few feet into the reservoir. Long well tests usually incorporate unavoidable flow variations. The detrimental effect of such variations can be eliminated through the use of the proposed deconvolution method.

Wellbore storage can mask the entire duration of well tests in high permeability wells. Since such reservoirs quickly transmit pressure transients, distant reservoir boundaries may be encountered before the wellbore storage effect has ended. If the sandface flow rate is known, the proposed method of deconvolution will unmask all wellbore storage effects and allow analysis of the well test data.

The proposed deconvolution method improves analysis of tests on wells that exhibit large wellbore storage coefficients. Wells in this category typically have a large tubing diameter and low fluid density (eg. high rate gas wells).

Deconvolving the pressure data with knowledge of the sandface flow rate enables analysis of early time data and shortens well tests considerably.

Dual porosity reservoirs are sometimes mistaken for single porosity systems because the secondary porosity pressure transient is masked by wellbore storage. Deconvolution can unmask the wellbore storage effect on early time data, making the secondary porosity system visible.

Sometimes it is not possible to achieve a long buildup period after a gas well modified isochronal deliverability test. This extended flow and buildup period is essential for assessing permeability and skin. Using the proposed method to deconvolve the short flow and shut-in periods of the isochronal test produces deconvolved drawdown data that can be analyzed for these reservoir parameters.

Finally, in horizontal wells the early radial and early linear flow periods can be masked by wellbore storage. However analyzing the early radial flow period is critical to the determination of vertical permeability (k_z) and skin. The longer wellbore of the horizontal well can contribute to a more pronounced wellbore storage affect. Deconvolving the pressure transient data using the proposed method can enable analysis of these early flow periods.

Chapter 6.

Conclusions

In order to continually produce revenue while well testing, operators of flowing oil and gas wells can replace popular buildup tests with drawdown tests that are analyzed using the proposed deconvolution method. Indeed, use of the method increases the scope of wells that can be practically tested to include wells that incur unavoidable flow rate changes, or have extended wellbore storage affects.

The method deconvolves bottom hole pressure data in conjunction with sandface flow rate data yielding the pressure influence function. Using the deconvolved data, well test analysts can more confidently identify the correct reservoir flow model and choose the appropriate analysis methods. Analysis using type curve or conventional techniques provides more accurate reservoir parameters when deconvolved test data are used rather than raw measured data.

The proposed deconvolution method is general in nature and easy to use. The method is reliable for any type of fluctuation in flow rate and a variety of reservoir flow types. It is equally suitable for radial, linear and spherical flow. It also successfully deconvolves well tests influenced by several different flow regimes. It unmasks various sandface flow rate schedules including linear increasing flow rates, rate changes caused by wellbore storage, multiple constant flow rates and periodically changing flow rates.

References Cited

1. Lee, W. John. Well Testing, SPE Textbook Series Volume 1. New York: SPE, 1982.

2. Jargon, J. R., and H. K. Van Poollen. "Unit Response From Varying-Rate Data." Journal of Petroleum Technology 17, no. 8 (Aug 1965): 965-969.

3. Gladfelter, R.E., G.W. Tracy, and L.E. Wilsey. "Selecting Wells Which Will Respond to Production-stimulation Treatment." Drilling and Production Practice, API (1955): 117-129.

4. Winestock, A.G. and G.P. Colpitts. "Advances in Estimating Gas Well Deliverability." Journal of Canadian Petroleum Technology 4, no. 2 (Jul. 1965): 111-119.

5. Kuchuk, F.J. "Gladfelter Deconvolution." SPE paper 16377, 1987: 499-509.

6. van Everdingen, A.F., and W. Hurst. "The Application of the Laplace Transformation to Flow Problems in Reservoirs." Petroleum Transactions, AIME 18, no. 6 (Dec. 1949): 305-324.

7. Kucuk, F., and L. Ayestaran. "Analysis of Simultaneously Measured Pressure and Sandface Flow Rate in Transient Well Testing." Journal of Petroleum Technology 37, no. 2 (Feb. 1985): 323-334.

8. Meunier, D., M. J. Wittmann, and G. Stewart. "Interpretation of Pressure Buildup Test Using In-Situ Measurement of Afterflow." Journal of Petroleum Technology 37, no. 1 (Jan. 1985): 143-152.

9. Hamming, R.W. Numerical Methods for Scientists and Engineers. 2nd ed. New York: McGraw, 1973: 375-377.

10. Kucuk, F., R. G. Carter, L. Ayestaran. "Numerical Deconvolution of Wellbore Pressure and Flow Rate." Unsolicited SPE Paper 13960 (Feb. 13, 1985).

11. Stanislav, J.F., and C.S. Kabir. Pressure Transient Analysis. Englewood, New Jersey: Prentice-Hall, 1990.

12. Streltsova, T.D. Well Testing in Heterogeneous Formations, An Exxon Monograph. New York: Wiley, 1988.

13. Craft, B.L., and M.F. Hawkins. Applied Petroleum Reservoir Engineering. Englewood Cliffs, New Jersey: Prentice Hall, 1959.

14. Odeh, A.S., and L.G. Jones. "Pressure Drawdown Analysis, Variable Rate Case." Journal of Petroleum Technology 17, no. 8 (Aug. 1965): 960-964.

15. Bourdet, D., J.A. Ayoub, and Y.M. Pirard. "Use of Pressure Derivative in Well-Test Interpretation." SPE Formation Evaluation 4, no. 2 (Jun. 1989): 293-302.

Appendix A.

Derivation of the Convolution Integral

Mathematical modelling of fluid flow through porous media is achieved by applying continuity of mass and momentum. The conservation of energy need not be considered except for those reservoirs being treated with a steam flood or in situ combustion. For single phase flow, the principle of conservation of mass states

$$\frac{\partial(\rho\phi)}{\partial t} = -(\nabla \cdot \rho \mathbf{v}) \qquad \text{A.1}$$

However, three distinct fluid phases may flow in hydrocarbon reservoirs namely, oil, gas and water. The principle of mass conservation for each phase follows the form

Oil

$$\frac{\partial}{\partial t}\left[\frac{1}{B_o}\phi S_o\right] + \nabla \cdot \left[\frac{1}{B_o}\mathbf{v}_o\right] + q_o = 0 \qquad \text{A.2}$$

Water

$$\frac{\partial}{\partial t}\left[\frac{1}{B_w}\phi S_w\right] + \nabla \cdot \left[\frac{1}{B_w}\mathbf{v}_w\right] + q_w = 0 \qquad \text{A.3}$$

Gas

$$\frac{\partial}{\partial t}\left[\phi\left[\frac{R_s}{B_o}S_o + \frac{1}{B_g}S_g\right]\right] + \nabla \cdot \left[\frac{R_s}{B_o}\mathbf{v}_o + \frac{1}{B_g}\mathbf{v}_g\right] + q_{fg} + R_s q_o = 0 \qquad \text{A.4}$$

where S_i, q_i and v_i are the saturation, flow rate and velocity of phase i in the porous media. The formation volume factor B_i is a ratio of the volume of phase i at reservoir conditions to the volume of the same mass of phase i at standard conditions. The solution gas/oil ratio R_s is the volume of gas liberated from one unit volume of oil [13].

A flow relationship such as the Navier-Stokes equation could be used to describe the conservation of momentum. However, forming the boundary conditions for solution of such an equation are impossible to describe due to the conplex geometry of flow though pore spaces. Rather, the empirical Darcy flow equation suggests

$$\mathbf{v} = -\frac{k}{\mu}(\nabla p + \rho g) \qquad \text{A.5}$$

where the velocity v is the defined as the volumetric flow rate per unit of cross section area of the porous medium. The proportionality constant k is known as the permeability of the porous medium. Combination of this equation with equation A.1 produces

$$\frac{\partial(\rho\phi)}{\partial t} = \nabla \cdot \left[\rho\frac{k}{\mu}(\nabla p + \rho g)\right] \qquad \text{A.6}$$

One further equation relating the unknowns p and ρ is needed. Liquid hydrocarbons often exhibit constant compressibility, which is defined by

$$c_f \equiv \frac{1}{\rho}\left[\frac{\partial \rho}{\partial p}\right]_T \qquad \text{A.7}$$

This definition may be integrated to obtain the needed relationship between p and ρ.

$$\rho = \rho^\circ \exp[c_f(p - p^\circ)] \qquad \text{A.8}$$

in which ρ° is fluid density at the standard pressure p°.

Assuming constant rock properties (k,ϕ), constant viscosity (μ), negligible gravitation effects and ignoring the square of the pressure gradient, the following homogeneous linear partial differential equation results

$$\frac{\partial p}{\partial t} = \frac{k}{\phi \mu c_t} \nabla^2 p \qquad \text{A.9}$$

in which c_t is the compressibility of the total system including fluid and rock matrix. Equation A.9 is known as the diffusivity equation. The preceding derivation follows the treatment in reference 11.

The solution of the diffusivity equation (in field units) for a constant sandface flow rate (q_{sf}) is

$$p_i - p_{wf}(t_D) = \frac{141.2 \mu q_{sf}}{kh} p_D(t_D) \qquad \text{A.10}$$

in which p_D is the pressure influence function which depends on the pattern of flow in the reservoir rock matrix. For example, the p_D for radial flow in the porous media to a wellbore of very small diameter can be approximated by a function related to the logarithm of time. The wellbore schematic diagram in Figure A-1 illustrates the variables of equation A.10. The pressure at the bottom of the wellbore, p_{wf}, is lower than p_i causing fluid flow through the porous media of the reservoir toward the wellbore. The flow at the interface of the reservoir rock and the wellbore is q_{sf}. The pressure at the top of the wellbore, p_{th}, is lower than p_{wf}. Since the fluids flowing in the wellbore are compressible, an abrupt change in the wellhead flow rate (q) is followed by a gradual change in q_{sf}. This lag in change of flow rate is known as the wellbore storage effect.

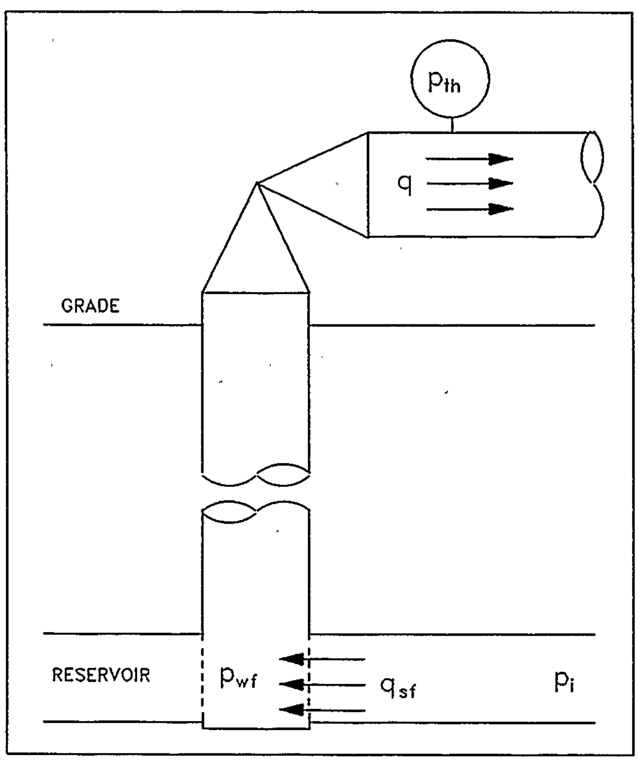

Figure A-1. Wellbore Schematic Diagram

Introducing the dimensionless variable q_D simplifies the mathematics of equation A.10.

$$q_D = \frac{q_{sf}}{q_{Ref}} \qquad \text{A.11}$$

where q_{Ref} is a reference sandface flow rate. Using this definition, the general form of solution for the flow equation becomes:

$$p_i - p_{wf}(t_D) = \frac{141.2\mu q_{Ref} q_D}{kh} p_D(t_D) \qquad \text{A.12}$$

The dimensionless variable p_{wDRef} is related to the bottom hole pressure difference via

$$p_{wDRef} = \frac{(p_i - p_{wf})kh}{141.2\mu q_{Ref}} \qquad \text{A.13}$$

Therefore, the dimensionless form of the diffusivity equation for a constant rate is

$$p_{wDRef}(t_D) = q_D p_D(t_D) \qquad \text{A.14}$$

For linear differential equations, such as equation A.9, the principle of superposition can be used to modify the solution for different boundary conditions. The principle of superposition for a two rate test would produce

$$p_{wDRef}(t_D) = q_{D1} p_D(t_D) + [q_{D2} - q_{D1}] p_D(t_D - t_{D1}) \qquad \text{A.15}$$

Where q_{D1} is the first rate, q_{D2} is the second rate, and t_{D1} is the time that the second rate begins. Using the principle of superposition for a test of N sandface flow rates:

$$p_{wDRef}(t_D) = \sum_{i=1}^{N} [q_{Di} - q_{D(i-1)}] p_D(t_D - t_{D(i-1)}) \tag{A.16}$$

Multiplying and dividing the flow equation by the quantity $(t_{Di} - t_{D(i-1)})$ produces

$$p_{wDRef}(t_D) = \sum_{i=1}^{N} \{[t_{Di} - t_{D(i-1)}]\left[\frac{q_{Di} - q_{D(i-1)}}{t_{Di} - t_{D(i-1)}}\right] \cdot p_D(t_D - t_{D(i-1)})\} \tag{A.17}$$

As the time increment becomes infinitesimally short the limit of the above equation is a form of the convolution integral [6].

$$p_{wDRef}(t_D) = \int_0^{t_D} \frac{dq_D(\tau)}{d\tau} p_D(t_D - \tau) d\tau \tag{A.18}$$

Another form of the integral can be derived through a change of variables:

$T = t_D - \tau$

$\tau = t_D - T$, and

$dT = -d\tau$.

When $\tau = t_D$, $T = 0$.

When $\tau = 0$, $T = t_D$.

Substituting this transformation into the integral equation produces

$$p_{wDRef}(t_D) = -\int_{t_D}^{0} \frac{dq_D(t_D - T)}{dT} p_D(T)\,dT \qquad \text{A.19}$$

Since T and τ are merely integration variables of convenience, they may be used interchangeably to produce

$$p_{wDRef}(t_D) = \int_{0}^{t_D} \frac{dq_D(t_D - \tau)}{d\tau} p_D(\tau)\,d\tau \qquad \text{A.20}$$

which is a second form of the convolution integral.

We may integrate this equation by parts to obtain another form. The principle of integration by parts is

$$\int_0^{t_D} u\,dv = \int_0^{t_D} d(uv) - \int_0^{t_D} v\,du$$

In this case, the following substitutions are made

$$u = p_D(\tau) \qquad du = \frac{dp_D(\tau)}{d\tau}d\tau$$

$$v = -q_D(t_D - \tau) \qquad dv = \frac{dq_D(t_D - \tau)}{d\tau}d\tau$$

to yield

$$p_{wDRef}(t_D) = -\,p_D(t_D)q_D(0) + p_D(0)q_D(t_D) + \int_0^{t_D} q_D(t_D - \tau)\frac{dp_D(\tau)}{d\tau}d\tau \qquad \text{A.21}$$

If both p_D and q_D disappear when $t_D = 0$, then the above formula becomes another form of the convolution integral.

$$p_{wDRef}(t_D) = \int_0^{t_D} q_D(t_D - \tau)\frac{dp_D(\tau)}{d\tau}d\tau \qquad \text{A.22}$$

Lastly, a change of variables similar to that used to produce Equation A.11 from Equation A.9 yields the fourth and final form of the integral.

$$p_{wDRef}(t_D) = \int_0^{t_D} q_D(\tau)\frac{dp_D(t_D - \tau)}{d\tau}d\tau \qquad \text{A.23}$$

Appendix B.

Continuous Convolution of Radial Flow with a Wellbore Storage Sandface Flow Schedule

An infinitely acting cylindrical reservoir in which radial flow occurs to a wellbore of infinitesimally small radius is usually modelled using the exponential integral solution or the log approximation to this solution [11]. When tested at a constant rate, the semi-log pressure derivative is a constant 0.5 as shown in Figure B-1.

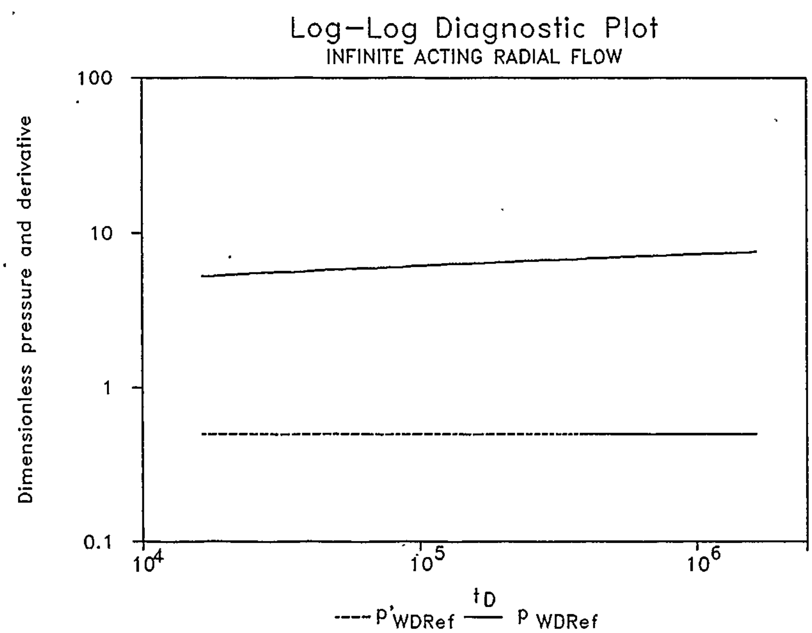

Figure B-1. Pressure Influence Function of a Well Test in which Fluids Flow Radially in the Reservoir

The log approximation of the exponential integral solution is usually expressed as

$$p_D = \frac{1}{2}\left[\ln\left(\frac{t_D}{r_D^2}\right) + 0.809\right] \qquad \text{B.1}$$

Table B.1. Reservoir Parameters Used to Model Synthetic Pressure Response in an Infinite Cylindrical Reservoir Produced at a Constant Flow Rate Affected by Wellbore Storage

Reservoir Parameter	Parameter Value	Units
k	12.	mD
h	10.	ft
μ	1.2	cp
r_w	0.40	ft
ϕ	10.%	
c_t	1.0e-5	1/psi
p_i	3000.	psia
q_{ref}	100.	STB/day
B_o	1.2	bbl/STB

For the synthetic well with parameters listed in Table B.1, the dimensionless bottom hole pressure from a constant rate drawdown test is

$$p_{wDRef} = \frac{1}{2}[\ln(16481.25t) + 0.809] \qquad \text{B.2}$$

The effect of wellbore storage on a constant rate test is sometimes modelled as exponentially increasing to a constant value. Although the wellhead flow valve is opened and the well is encouraged to produce at a constant rate, there is some delay in the sandface flow rate as the fluids in the wellbore unload to the production tank. For the synthetic well test examined in this section, the sandface flow rate is displayed in Figure B-2 and mathematically modelled as

$$q(t) = 120(1 - e^{-0.3t}) \qquad \text{B.3}$$

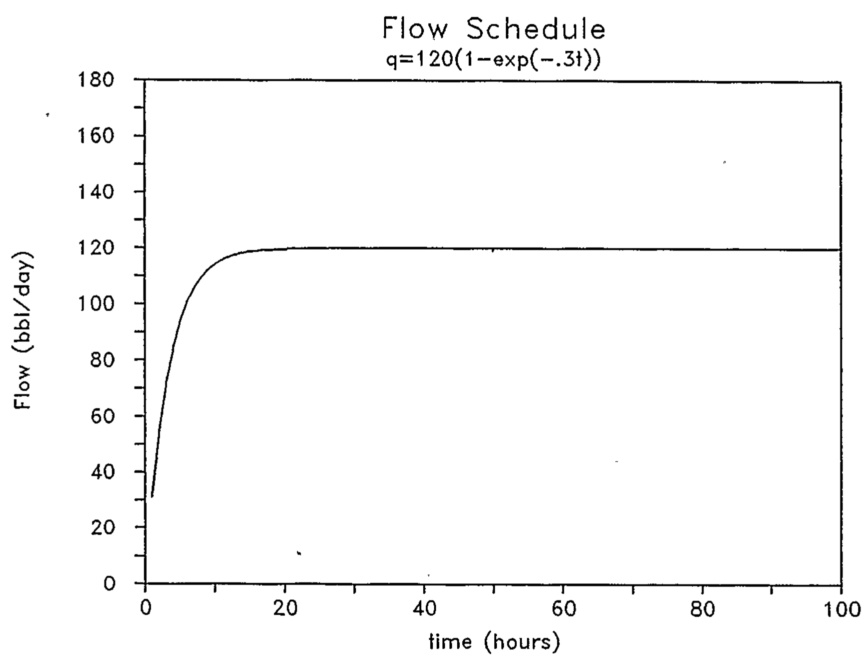

Figure B-2. Flow Rate Exponentially Increasing to a Constant Value

The drawdown test was conducted on the synthetic well defined by the parameters in Table B.1. Streltsova [12] found that when the wellbore radius r_w and the time constant of the exponential flow schedule are both small, the bottom hole pressure response of the well follows

$$p_{wf}(t) = 3000 - 84.72(1 - e^{-0.3t}) \cdot (\ln(16481.25t) + 0.809) \qquad \text{B.4}$$

Expressed as a dimensionless variable, the bottom hole pressure becomes

$$p_{wDRef} = \frac{1}{2}(1 - e^{-0.3t})(\ln(16481.25t) + 0.809) \qquad \text{B.5}$$

Using the deconvolution algorithm of Figure 3-1 on page 22, this synthetic well test was successfully deconvolved. The stages of the simulation are detailed pictorially in Appendix D.

Appendix C.

Continuous Convolution of Linear Flow with a Wellbore Storage Sandface Flow Schedule

In order to be useful, the proposed deconvolution method must be able to deconvolve any reservoir flow model. To approximate a well test of a fractured well, the linear flow model was continuously convolved with the wellbore storage sandface flow rate schedule using equation 2.1. The integration required is detailed in this section.

The wellbore storage sandface flow rate is expressed as

$$q(t) = 120(1 - e^{-0.3t}) \qquad \text{C.1}$$

which can be expressed in dimensionless terms by

$$q_D(t) = \frac{120}{q_{ref}}(1 - e^{-0.3t}) \qquad \text{C.2}$$

Differentiating with respect to time produces

$$q'_D(t) = \frac{36}{q_{ref}} e^{-0.3t} \qquad \text{C.3}$$

Using the reservoir parameters in Table 4.2 on page 27, the pressure influence function is

$$p_D(t) = 3.641\sqrt{t} \qquad \text{C.4}$$

or

$$p_D(t-\tau) = 3.641\sqrt{t-\tau} \qquad \text{C.5}$$

Substituting equations C.3 and C.5 into the convolution integral (Equation 2.1 on page 5) produces

$$p_{wDRef}(t) = \int_0^t \frac{36}{q_{ref}} e^{-0.3\tau} 3.641\sqrt{t-\tau}\,d\tau \qquad \text{C.6}$$

The binomial theorem states

$$(x+y)^n = x^n + nx^{n-1}y + \ldots \qquad \text{C.7}$$

which can be used to simplify the dimensionless pressure portion of the integrand of Equation C.6. Using the first two terms of the binomial theorem produces

$$(t-\tau)^{1/2} = t^{1/2} - \frac{\tau}{2t^{1/2}} \qquad \text{C.8}$$

Equation C.6 thus becomes

$$p_{wDRef}(t) = \int_0^t \frac{36}{q_{ref}} e^{-0.3\tau} 3.641\left(\sqrt{t} - \frac{\tau}{2\sqrt{t}}\right) d\tau \qquad \text{C.9}$$

or

$$p_{wDRef}(t) = \frac{36(3.641)\sqrt{t}}{q_{ref}} \int_0^t e^{-0.3\tau}\,d\tau - \frac{36(3.641)}{2q_{ref}\sqrt{t}} \int_0^t \tau e^{-0.3\tau}\,d\tau \qquad \text{C.10}$$

Integrating provides

$$p_{wDRef}(t) = \frac{36(3.641)\sqrt{t}}{q_{ref}}\left(1 - e^{-0.3\tau}\right) - \frac{36(3.641)}{2(0.3^2)q_{ref}\sqrt{t}}\left(1 - e^{-0.3\tau}[0.3t+1]\right) \qquad \text{C.11}$$

which simplifies to

$$p_{wDRef}(t) = \frac{436.92\sqrt{t}}{q_{ref}}(1 - e^{-0.3\tau}) - \frac{728.20}{q_{ref}\sqrt{t}}(1 - e^{-0.3\tau}[0.3t + 1]) \tag{C.12}$$

Equation C.12 was used to generate the bottom hole pressure data of the synthetic wellbore storage masked well test in simulation case B3C. The bottom hole pressure data was then deconvolved using the algorithm in Figure 3-1 on page 22. The deconvolution was quite successful as shown in the graphical comparison of Figure 4-10 on page 40. A pictorial history of the entire simulation is recorded in Appendix D.

Appendix D.

Pictorial Results From Simulations

The proposed deconvolution method makes pressure derivatives recognizable on a diagnostic plot. When tested at a varying flow rate, a log-log plot of raw bottom hole pressure derivatives rarely afford much information. However, after deconvolution, the applicable reservoir models become obvious. The advantage of deconvolution is apparent from the figures included in this Appendix which show the simulations used to test the proposed deconvolution method.

Each figure includes four graphs which document the stages of each simulation. The pressure influence function and flow schedule as well as the bottom hole pressure response that was obtained by convolution are displayed. Then the proposed deconvolution method was used to deconvolve the bottom hole pressure response, the results of which are also shown as the final plot of each figure.

In all cases, the deconvolved pressure response compares closely with the pressure influence function. The pictorial histories also show that the convolved pressure response would be difficult to analyze without deconvolution. The derivative curves for each of the convolved bottom hole pressure graphs were calculated using the forward difference algorithm which tends to underestimate the derivative of the pressure influence functions.

For a description of each simulation case, please refer to Table 4.4 on page 38.

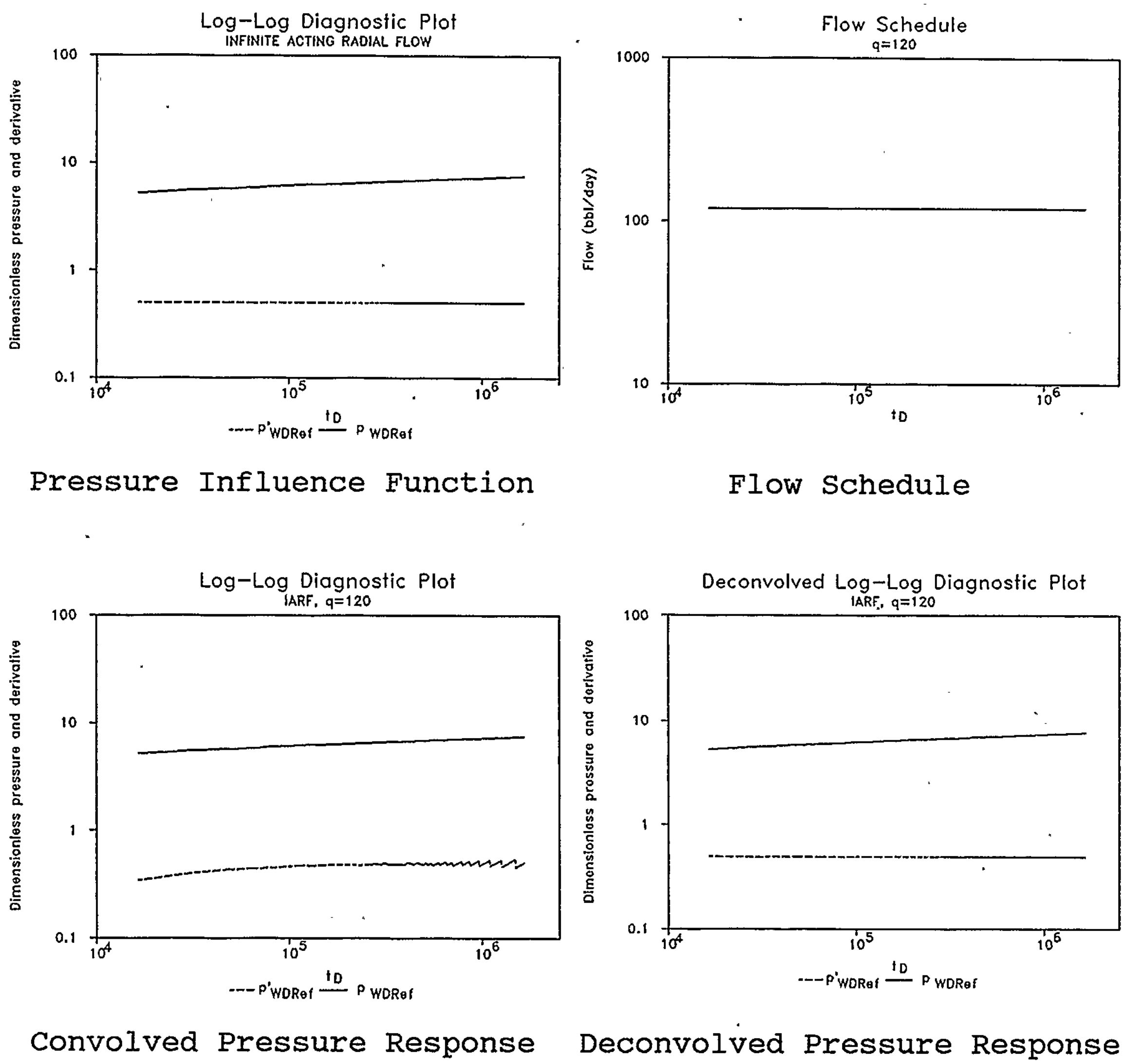

Figure D-1. Graphical History of Simulation Case A1.

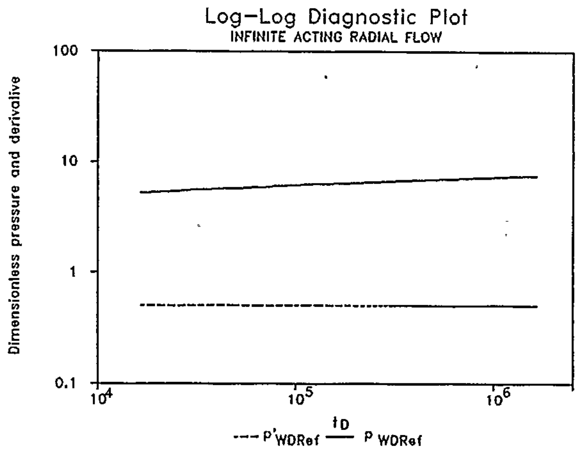

Pressure Influence Function

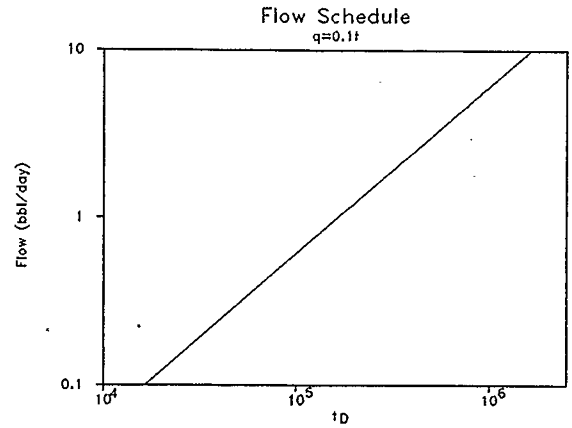

Flow Schedule

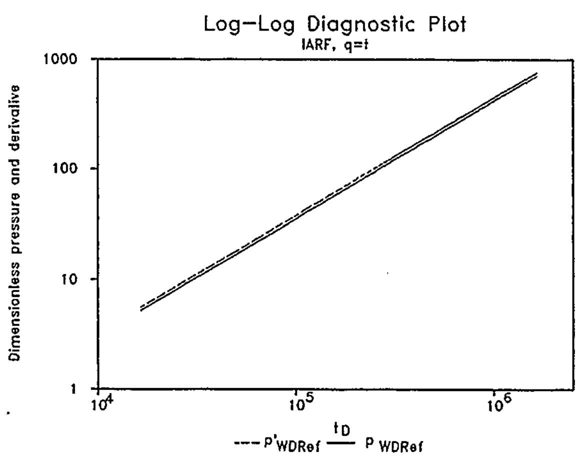

Convolved Pressure Response

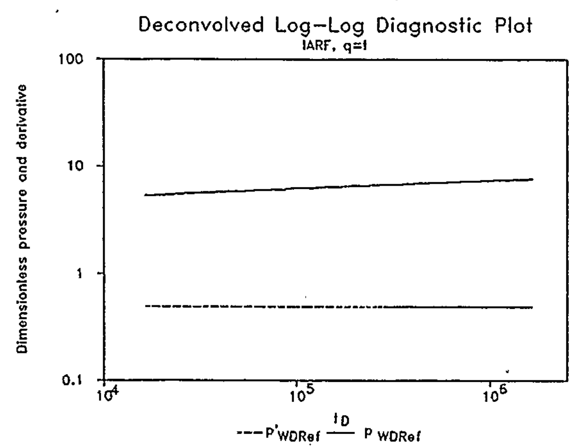

Deconvolved Pressure Response

Figure D-2. Graphical History of Simulation Case A2.

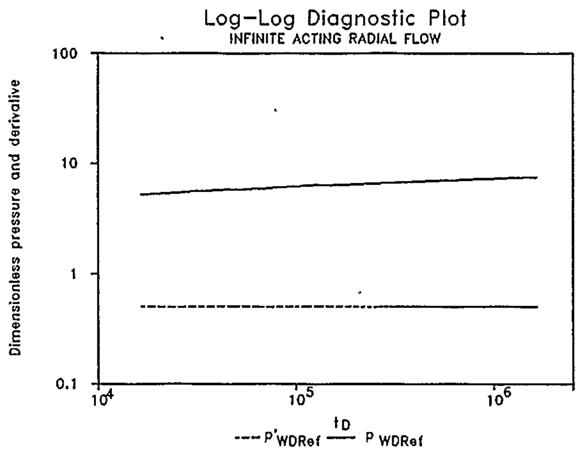

Pressure Influence Function

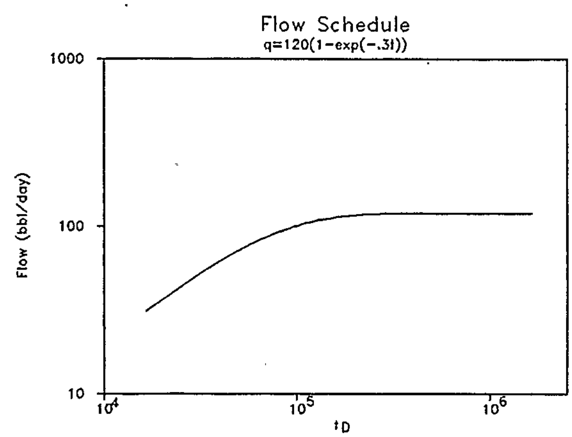

Flow Schedule

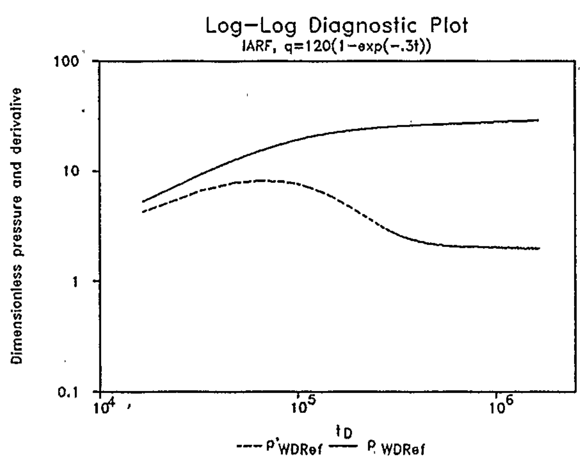

Convolved Pressure Response

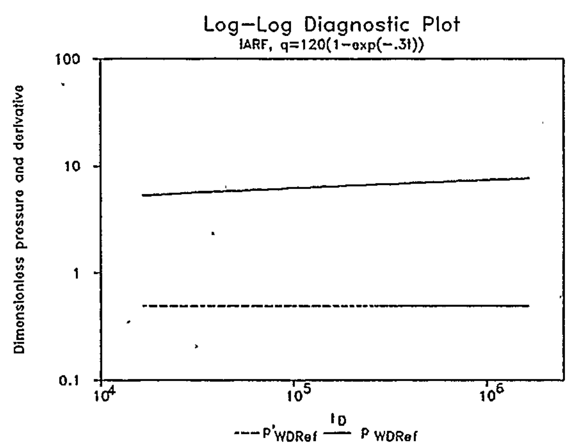

Deconvolved Pressure Response

Figure D-3. Graphical History of Simulation Case A3.

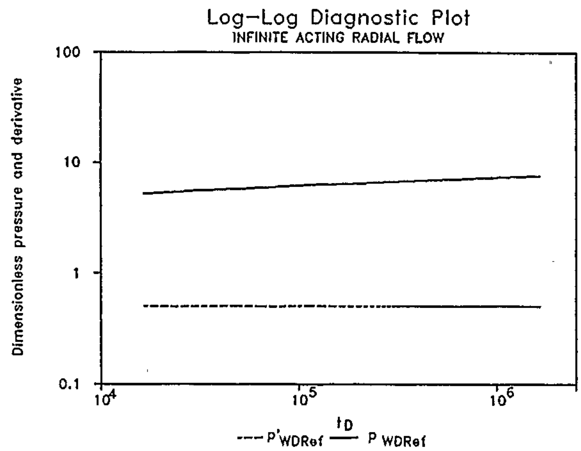

Pressure Influence Function

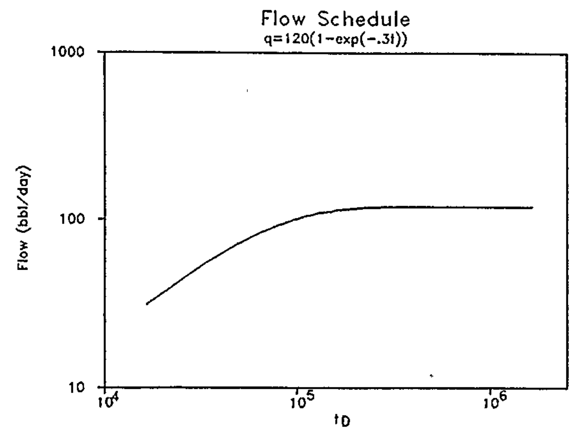

Flow Schedule

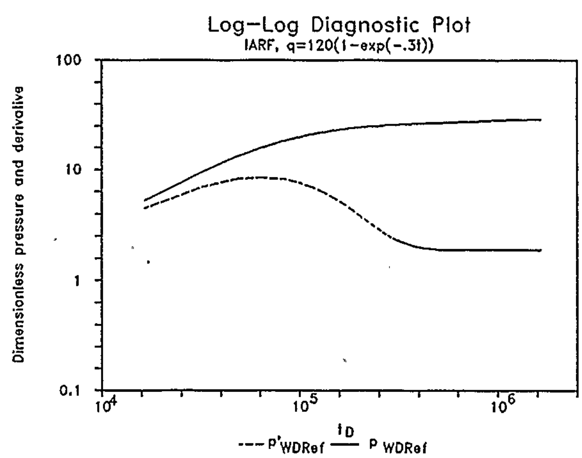

Convolved Pressure Response

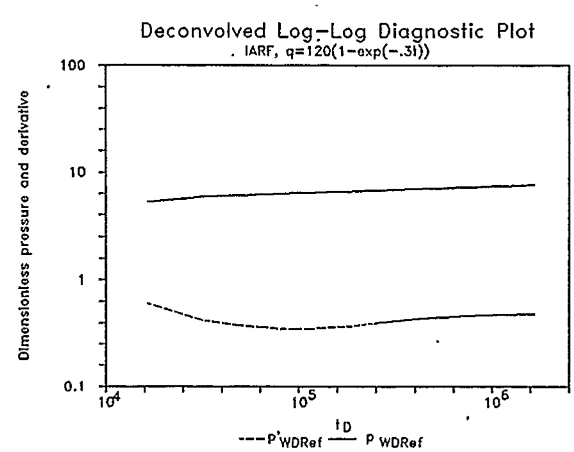

Deconvolved Pressure Response

Figure D-4. Graphical History of Simulation Case A3C.

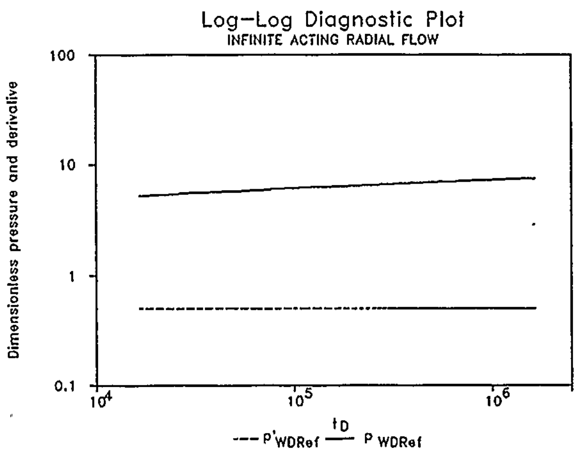

Pressure Influence Function

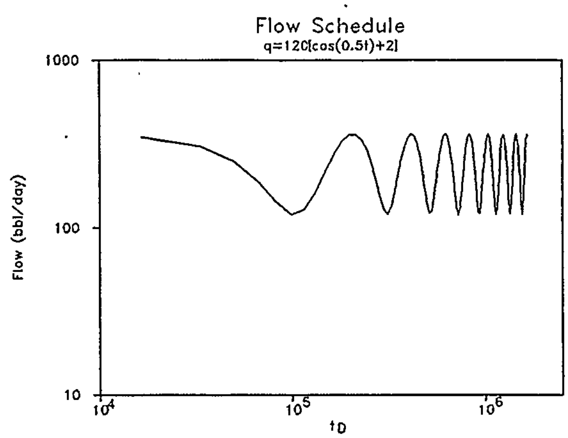

Flow Schedule

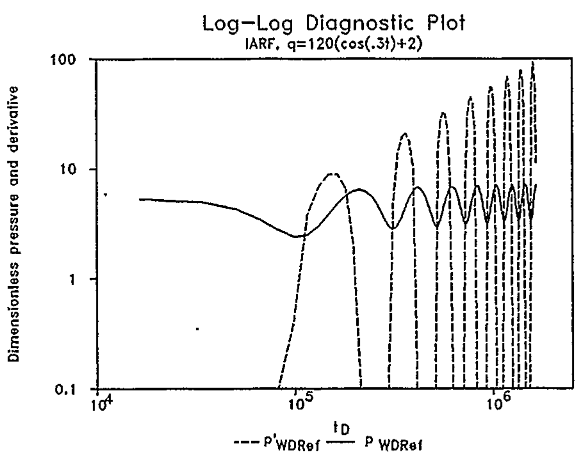

Convolved Pressure Response

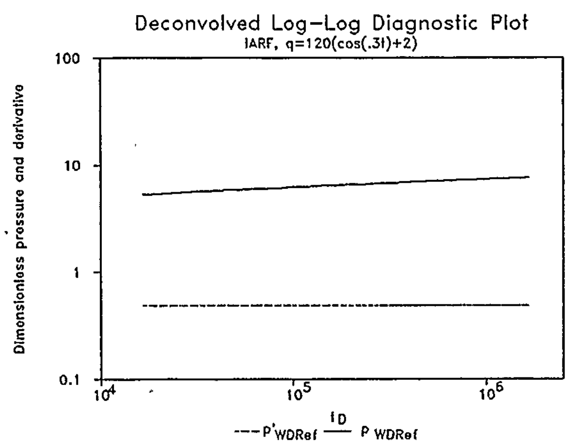

Deconvolved Pressure Response

Figure D-5. Graphical History of Simulation Case A4.

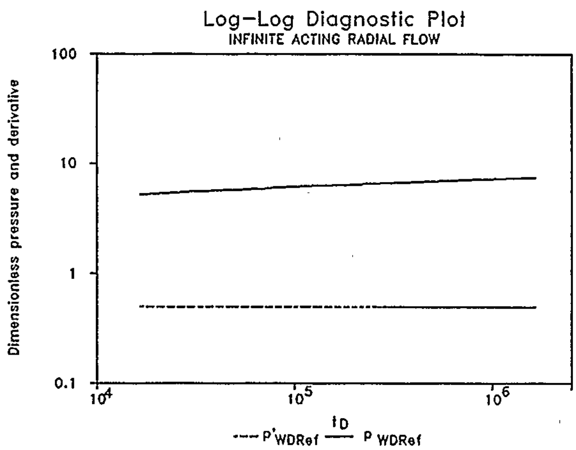

Pressure Influence Function

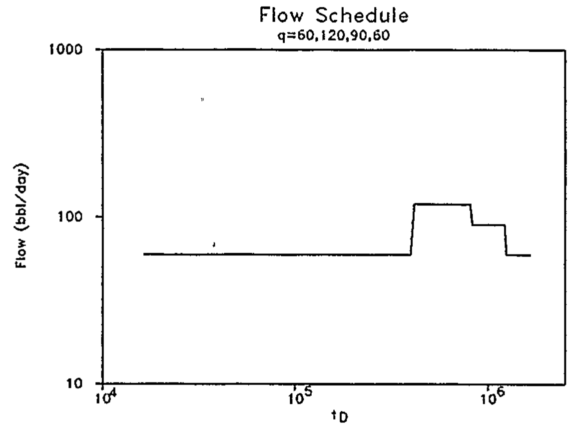

Flow Schedule

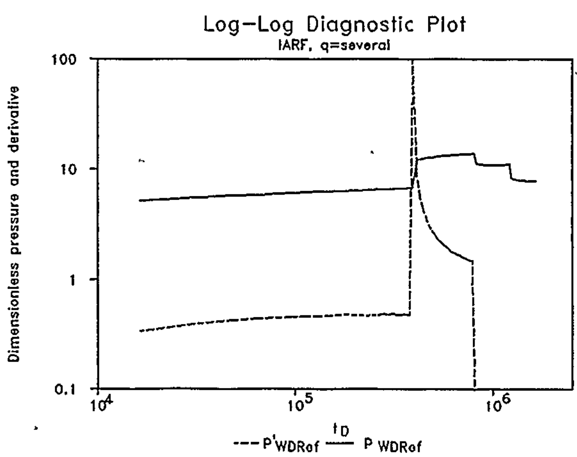

Convolved Pressure Response

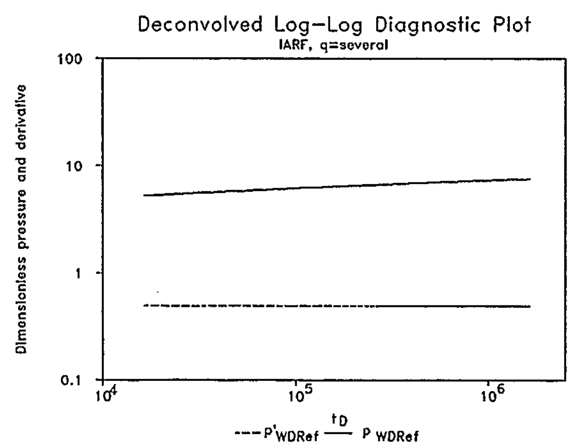

Deconvolved Pressure Response

Figure D-6. Graphical History of Simulation Case A5.

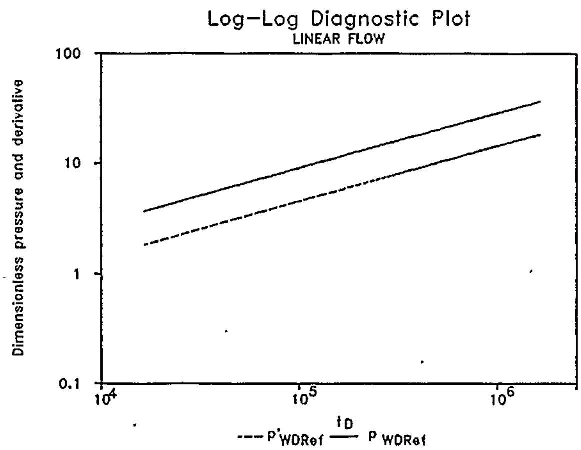

Pressure Influence Function

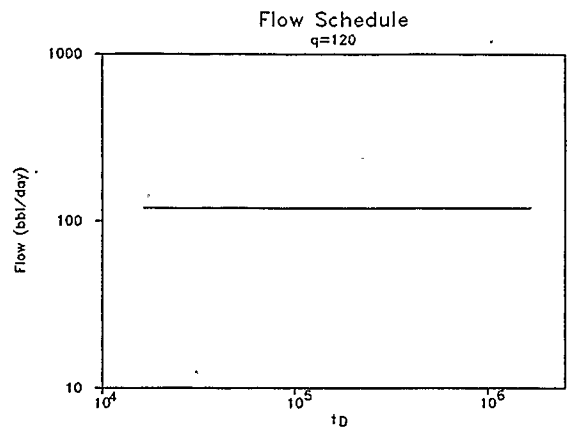

Flow Schedule

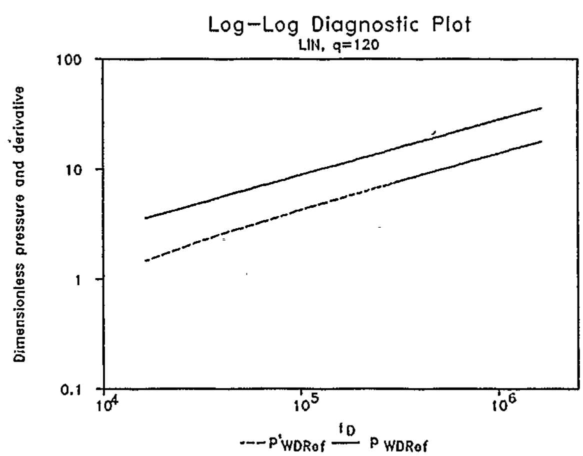

Convolved Pressure Response

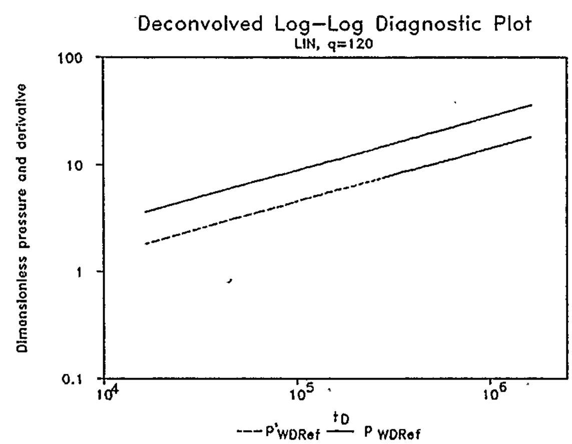

Deconvolved Pressure Response

Figure D-7. Graphical History of Simulation Case B1.

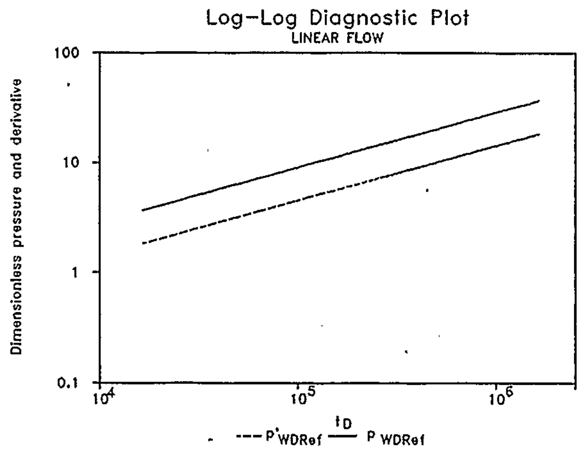

Pressure Influence Function

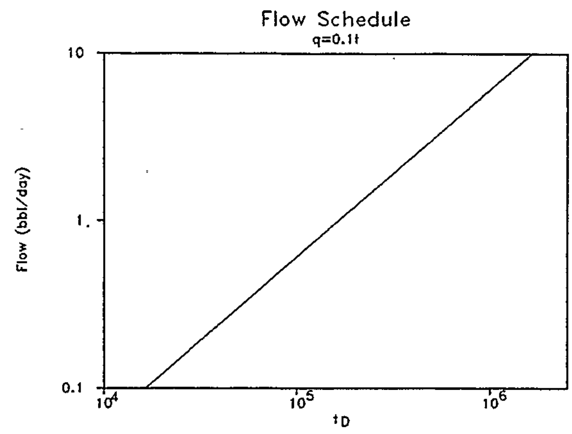

Flow Schedule

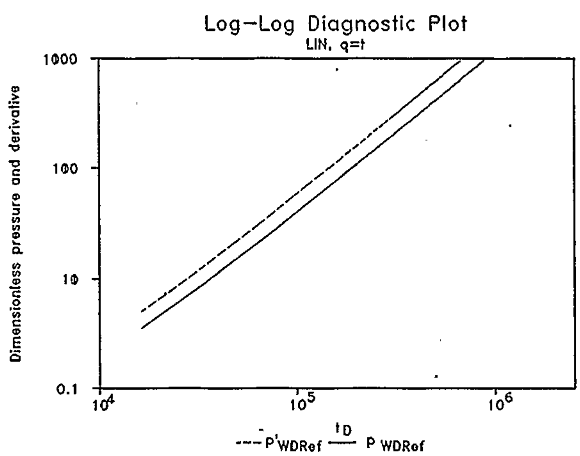

Convolved Pressure Response

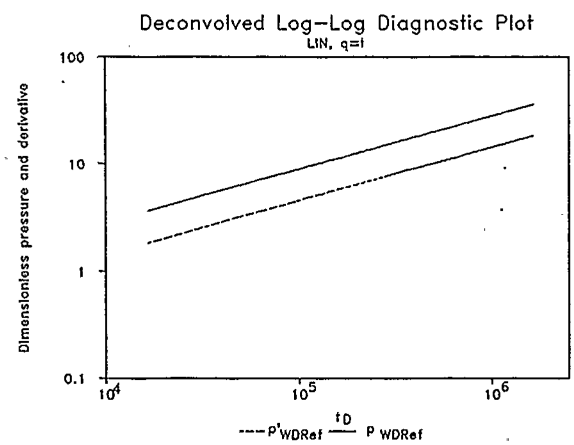

Deconvolved Pressure Response

Figure D-8. Graphical History of Simulation Case B2.

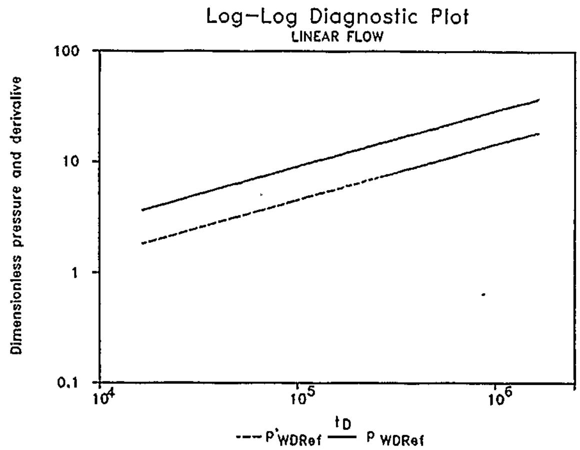

Pressure Influence Function

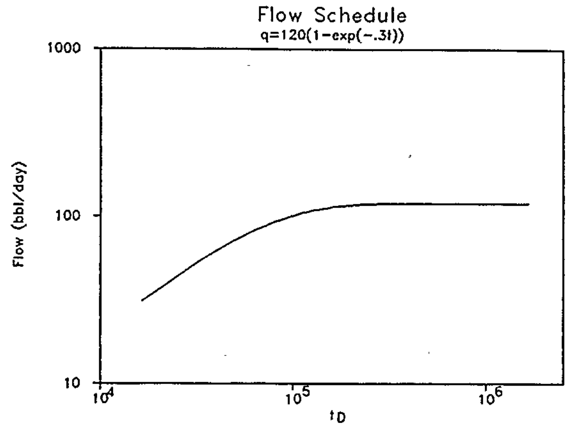

Flow Schedule

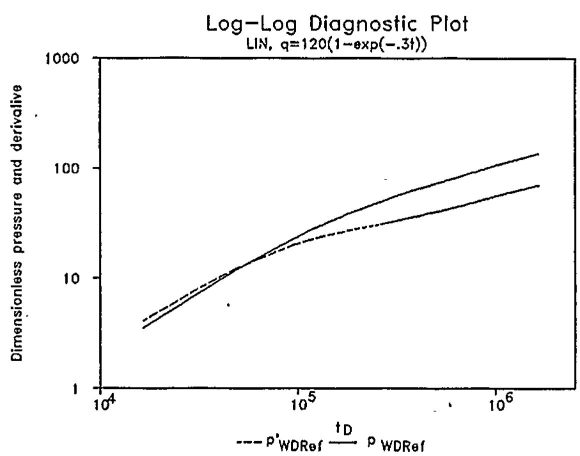

Convolved Pressure Response

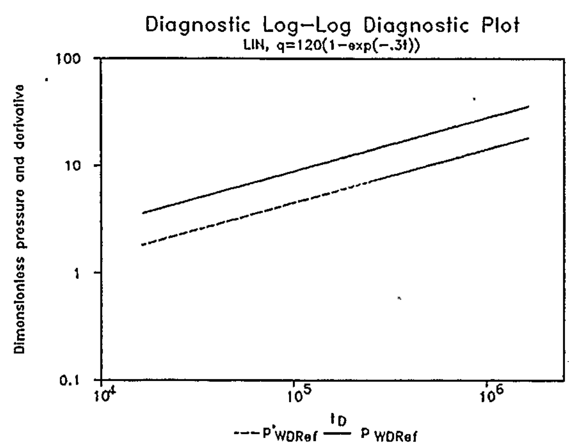

Deconvolved Pressure Response

Figure D-9. Graphical History of Simulation Case B3.

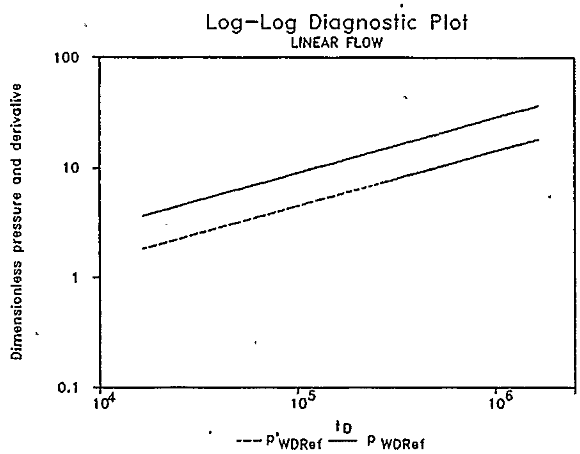

Pressure Influence Function

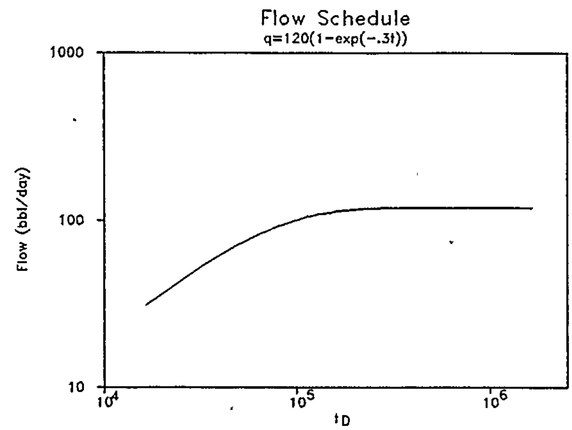

Flow Schedule

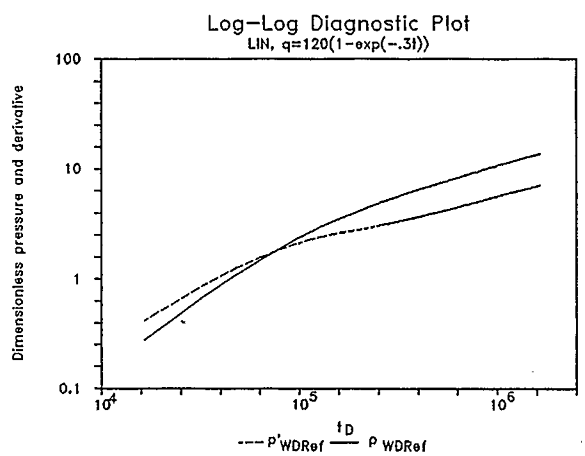

Convolved Pressure Response

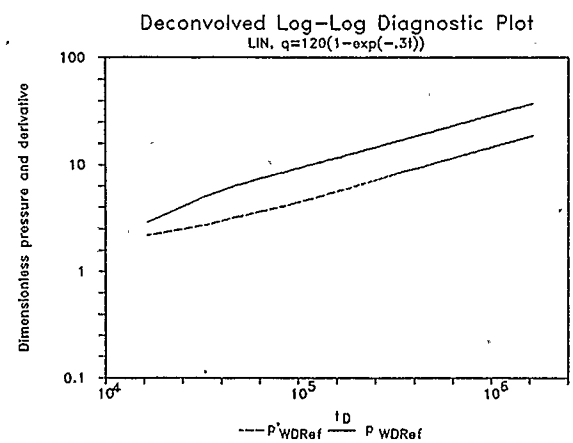

Deconvolved Pressure Response

Figure D-10. Graphical History of Simulation Case B3C.

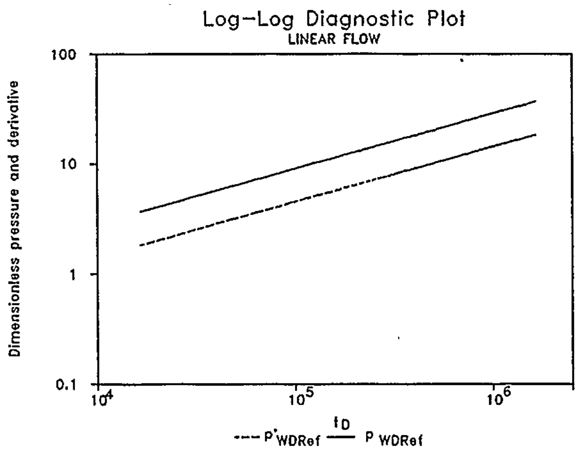

Pressure Influence Function

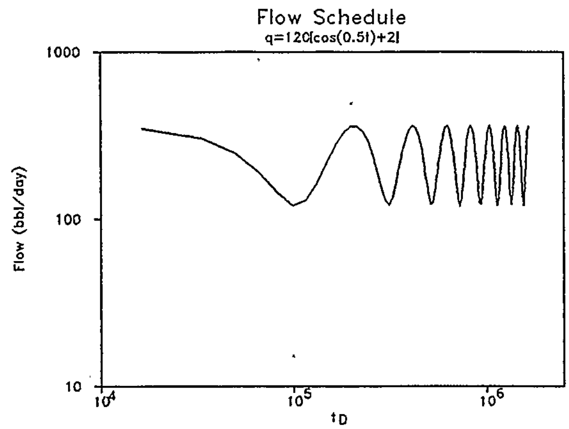

Flow Schedule

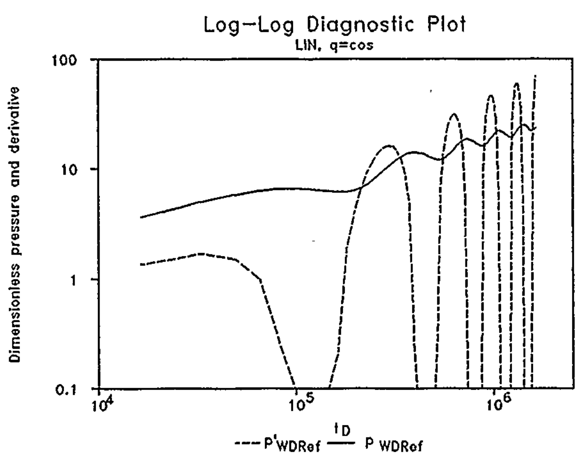

Convolved Pressure Response

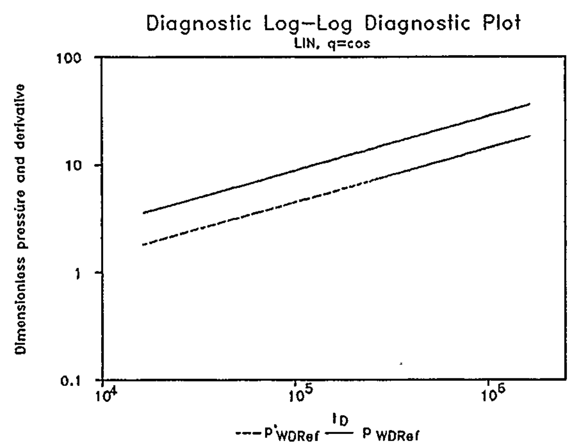

Deconvolved Pressure Response

Figure D-11. Graphical History of Simulation Case B4.

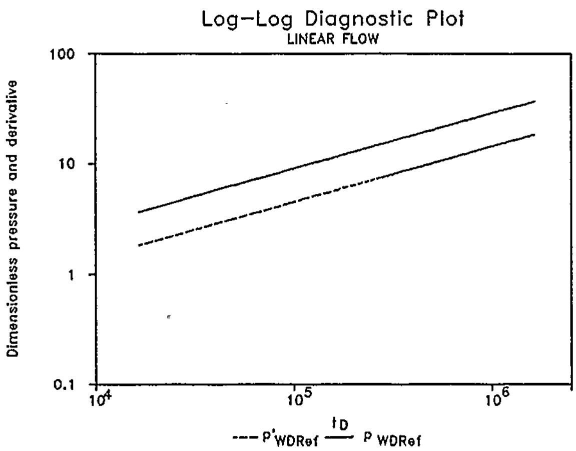

Pressure Influence Function

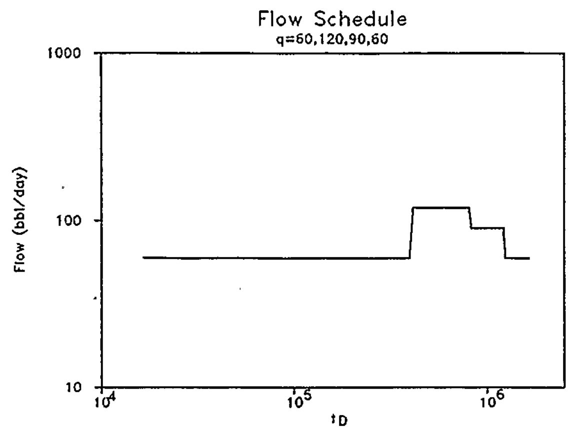

Flow Schedule

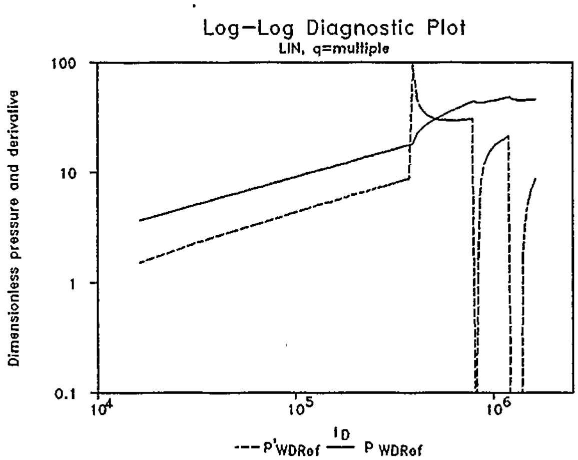

Convolved Pressure Response

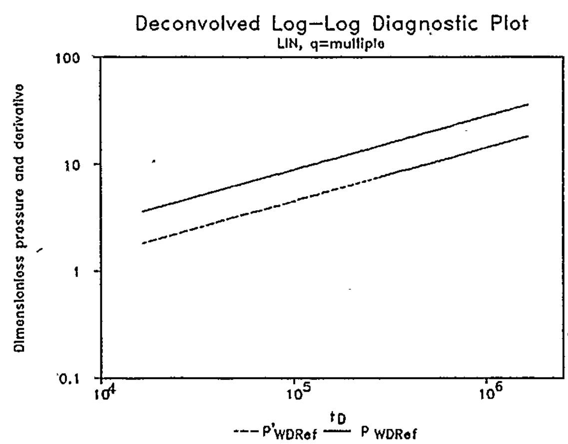

Deconvolved Pressure Response

Figure D-12. Graphical History of Simulation Case B5.

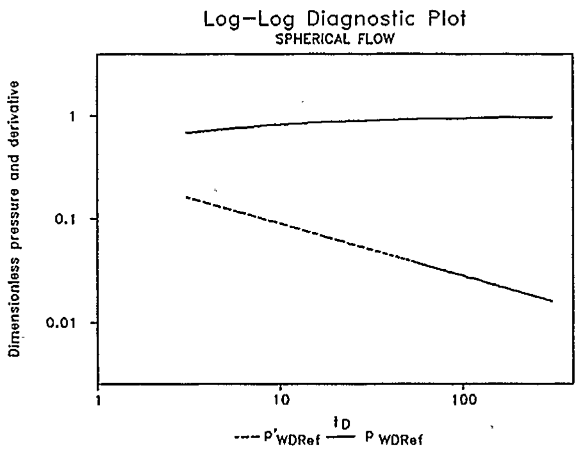

Pressure Influence Function

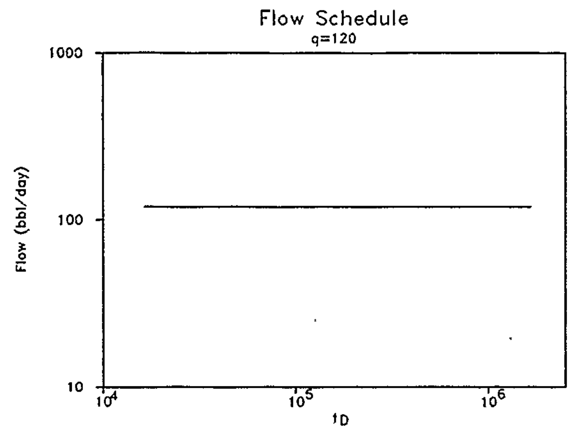

Flow Schedule

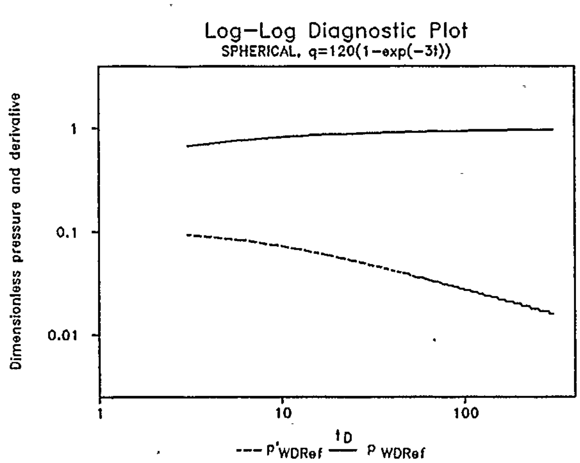

Convolved Pressure Response

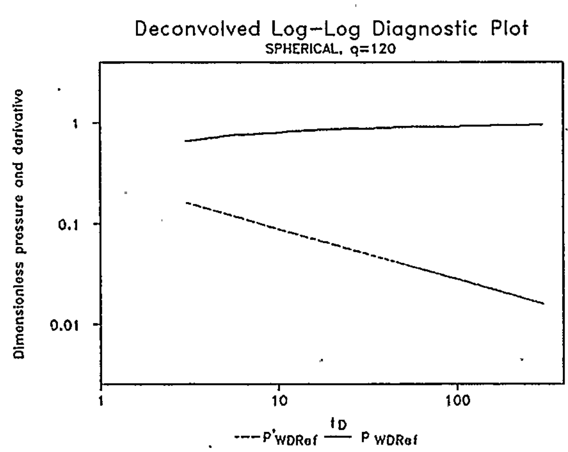

Deconvolved Pressure Response

Figure D-13. Graphical History of Simulation Case C1.

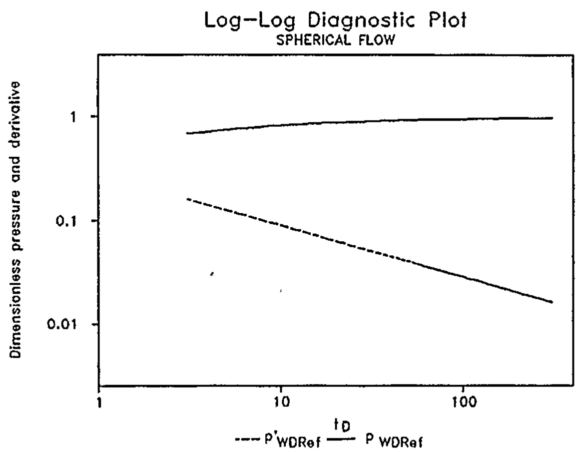

Pressure Influence Function

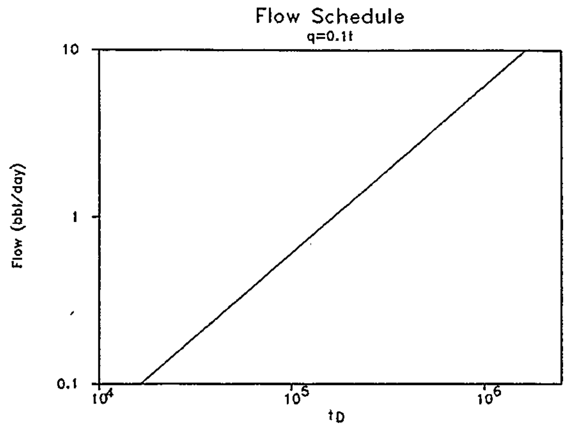

Flow Schedule

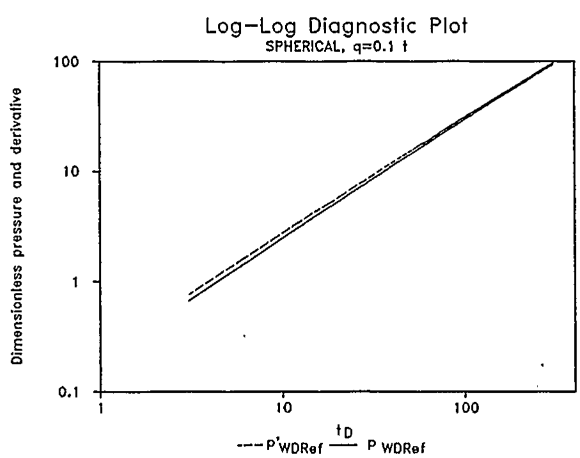

Convolved Pressure Response

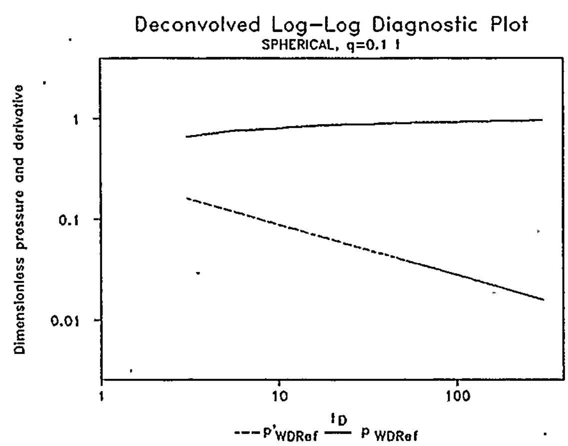

Deconvolved Pressure Response

Figure D-14. Graphical History of Simulation Case C2.

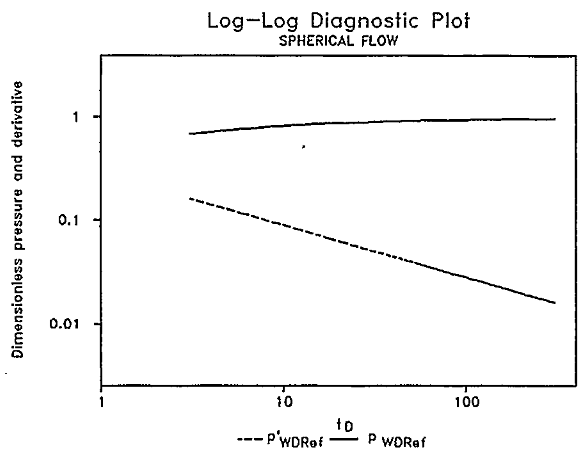

Pressure Influence Function

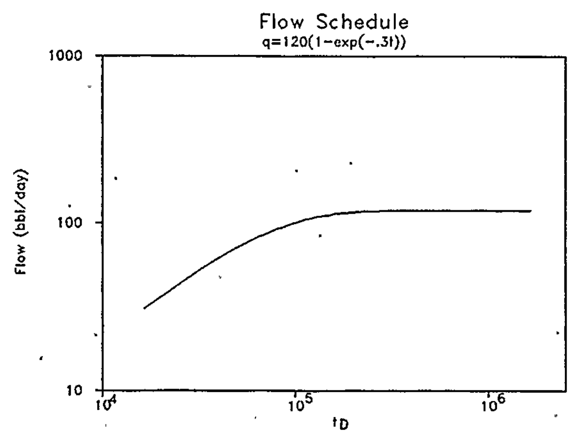

Flow Schedule

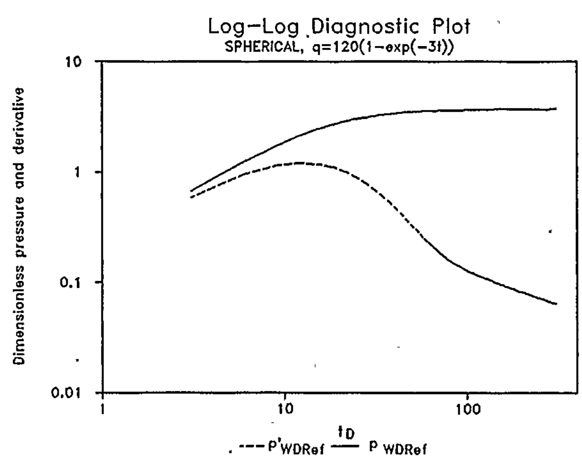

Convolved Pressure Response

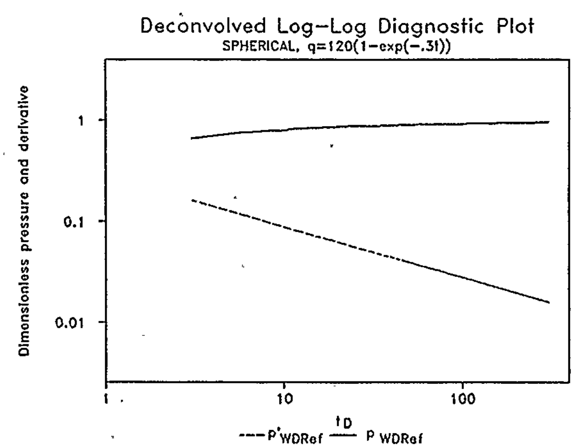

Deconvolved Pressure Response

Figure D-15. Graphical History of Simulation Case C3.

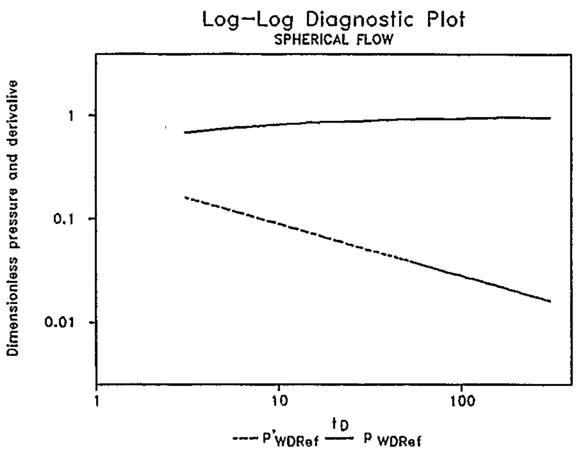

Pressure Influence Function

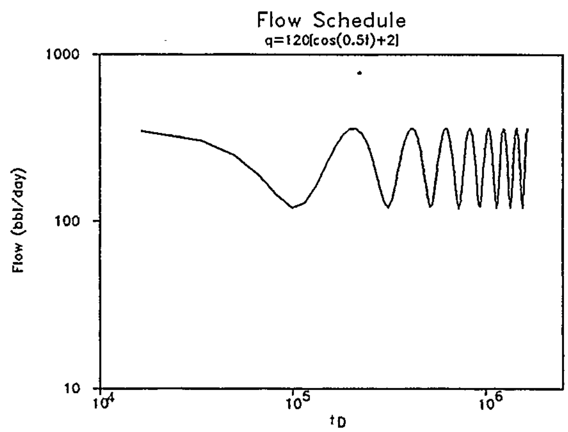

Flow Schedule

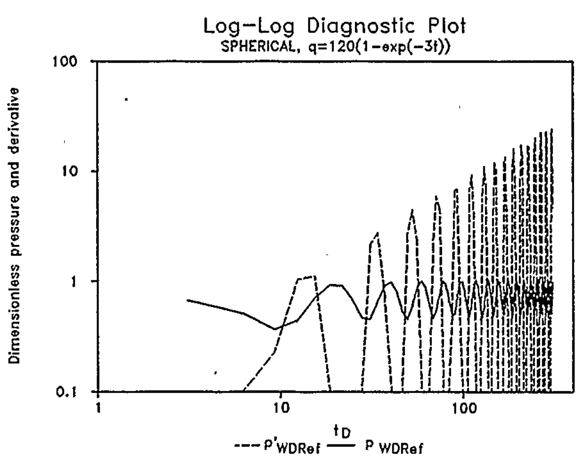

Convolved Pressure Response

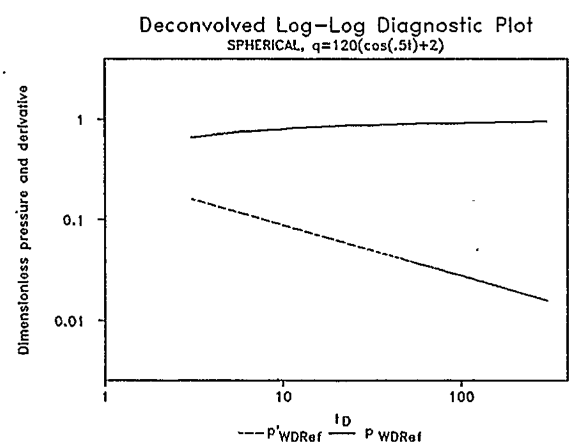

Deconvolved Pressure Response

Figure D-16. Graphical History of Simulation Case C4.

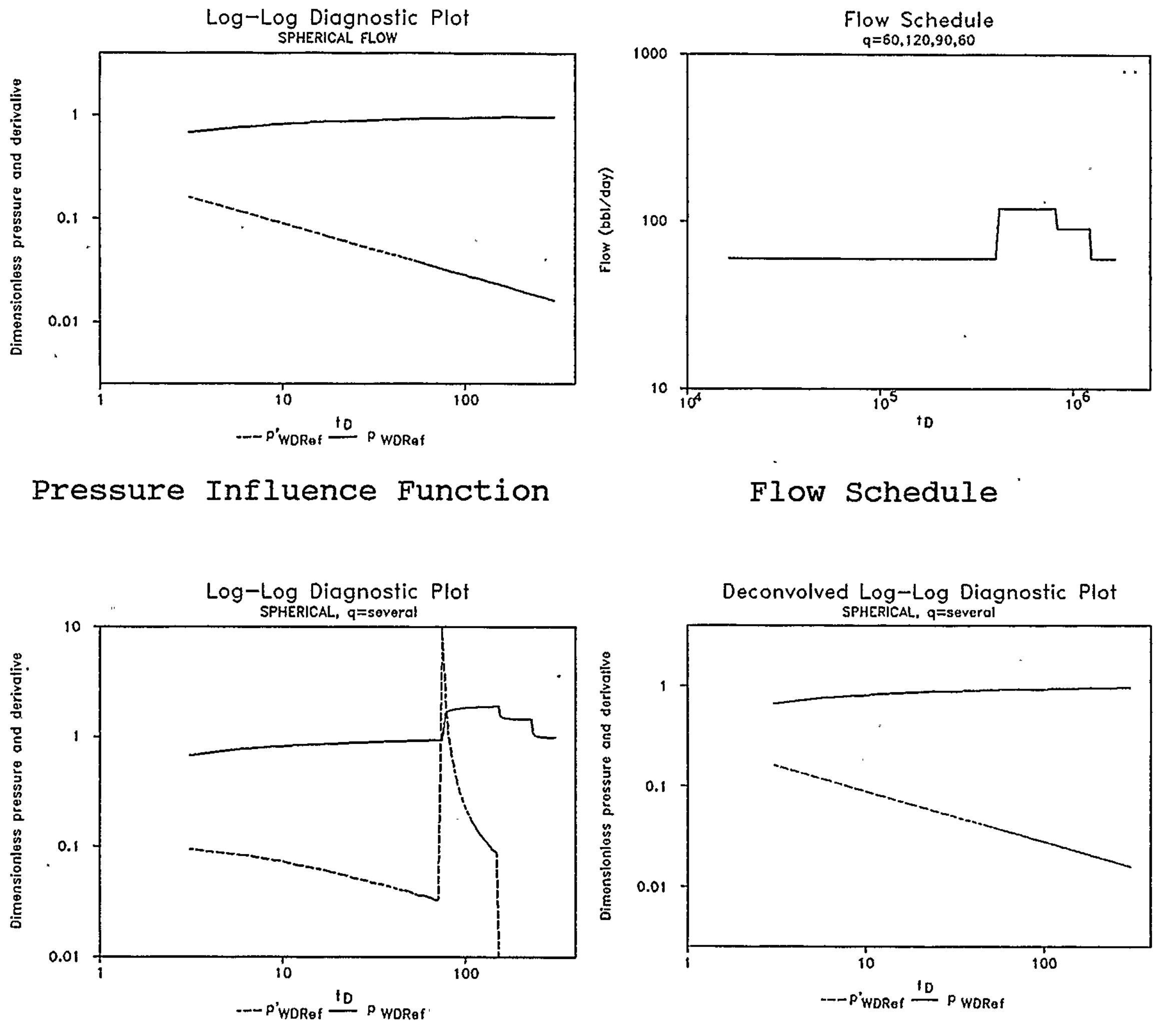

Pressure Influence Function

Flow Schedule

Convolved Pressure Response

Deconvolved Pressure Response

Figure D-17. Graphical History of Simulation Case C5.

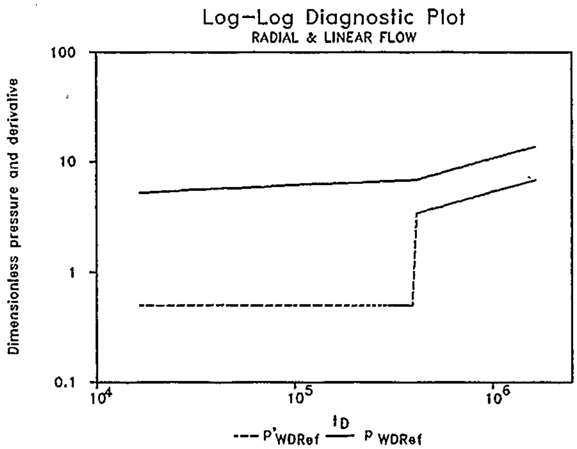

Pressure Influence Function

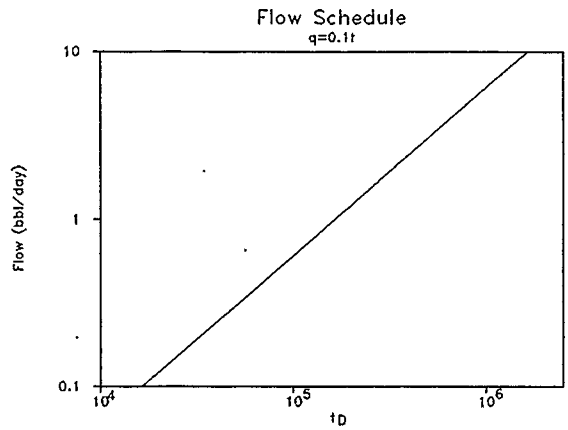

Flow Schedule

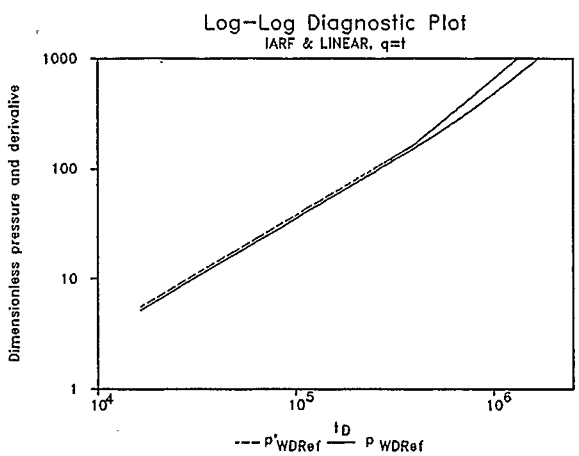

Convolved Pressure Response

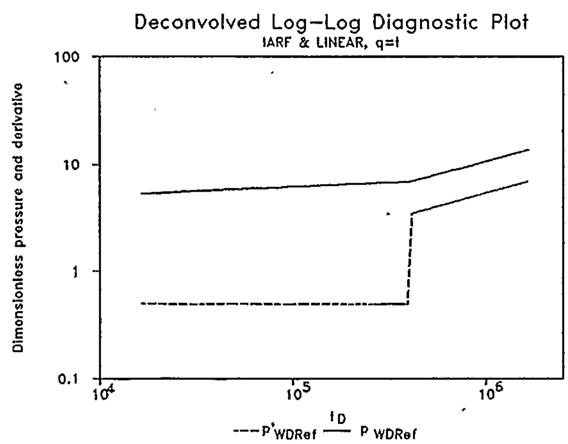

Deconvolved Pressure Response

Figure D-18. Graphical History of Simulation Case D2.

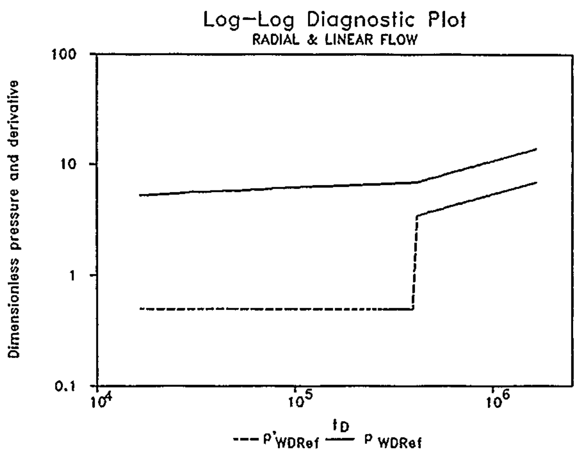

Pressure Influence Function

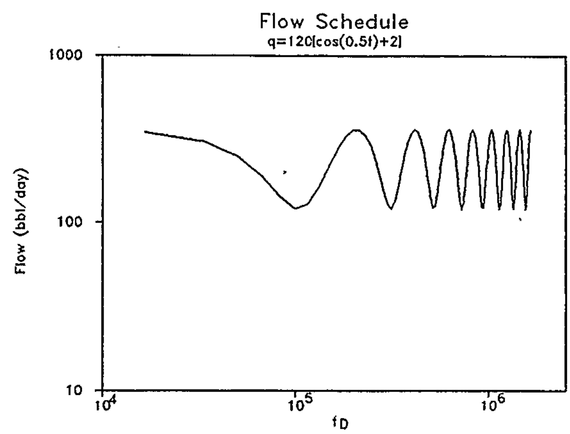

Flow Schedule

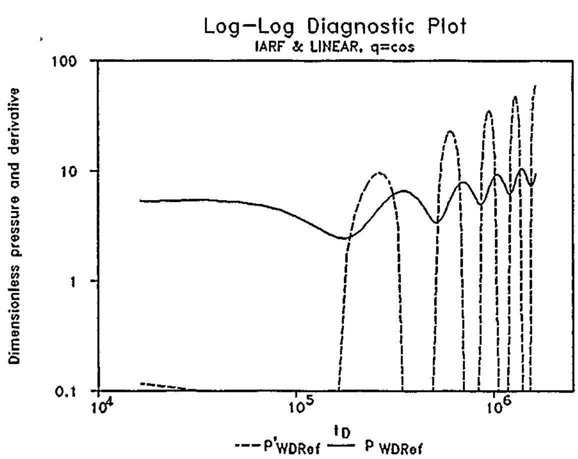

Convolved Pressure Response

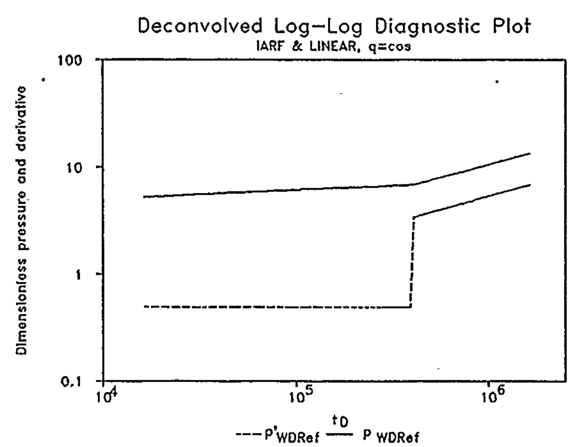

Deconvolved Pressure Response

Figure D-19. Graphical History of Simulation Case D4.

Appendix E.

Lee's Varying Rate Well Test Example

This appendix documents the deconvolution of the following example from Lee [1].

> "The data in Table E.1 were obtained in a drawdown test in which the rate was measured as a function of time. Other data include the following:"

$B = 1.136$ bbl/STB,
$\mu = 0.8$ cp,
$h = 69$ ft,
$\rho = 53$ lb/cu ft,
$A_{wb} = 0.0218$ sq ft,
$\phi = 0.039$,
$c_t = 17 \times 10^{-6}$ 1/psi
$r_w = 0.198$ ft

Table E.1. Measured Bottom Hole Pressure and Sandface Flow Rate Data for Lee's Varying Rate Well Test [1]

t (hours)	p_{wf} (psi)	q (STB/d)	t (hours)	p_{wf} (psi)	q (STB/d)
0	4412	250	8.32	3927	147
0.105	4332	180	9.99	3928	145
0.151	4302	177	14.4	3931	143
0.217	4264	174	20.7	3934	140
0.313	4216	172	29.8	3937	137
0.45	4160	169	43	3941	134
0.648	4099	166	61.8	3944	132
0.934	4039	163	74.2	3946	130
1.34	3987	161	89.1	3948	129
1.94	3952	158	107.	3950	127
2.79	3933	155	128.	3952	126
4.01	3926	152	154.	3954	125
5.78	3926	150	185.	3956	123

<u>1. Interpolate Data Points at Equal Time Steps.</u> The first step is to calculate evenly spaced data from the measured data using linear interpolation. A time time step of 1 hour was used. The pressure difference $p_i - p_{wf}$ was also calculated at each evenly spaced time step.

<u>2. Deconvolve.</u> The algorithm of Figure 3-1 on page 22 was used to deconvolve the evenly spaced data.

<u>3. Log-log Diagnostic Plot.</u> The log-log plot of the deconvolved pressure vs time aids in identifying the middle time region from which the reservoir parameters will be calculated. From Figure 4-13 on page 43, it can be seen that the early time region ends at about 4 hours. From the plot of the deconvolved data, infinite homgeneous radial flow is evident throughout the test.

<u>4. Semi-log Plot.</u> A semi-log plot of the well's deconvolved pressure vs time is then used to find a slope of 48.5 psi/cycle (see Figure 4-14 on page 43).

<u>5. Calculate Reservoir Parameters.</u> Using the equation

$$\hat{p}_{wf} = p_i + 162.6\frac{qB\mu}{kh}\left[\log\left(\frac{1688\phi\mu c_t r_w^2}{kt}\right) - 0.869s\right] \tag{E.1}$$

the slope may be found

$$m = 162.6\frac{qB\mu}{kh} = 48.5 \tag{E.2}$$

Rearranging to solve for permeability,

$$k = 162.6\frac{q_{ref}B\mu}{mh} = 7.18mD \qquad \text{E.3}$$

The equation for calculating skin is

$$s = 1.151\left(\frac{p_i - \hat{p}_{1hr}}{m} - \log\left(\frac{k}{\phi\mu c_t r_w^2}\right) + 3.23\right) \qquad \text{E.4}$$

From Figure 4-14 it is found that $\hat{p}_{1hr}$ is 3922 psig. Substituting this value into the above equation produces a skin of 5.52.

Both permeability and skin calculated with this method are very similar to those calculated by Lee. Using a different method, he calculated

$$k = 7.44mD \qquad \text{E.5}$$

$$s = 6.02$$

Appendix F. Odeh and Jones' Three Rate Well Test

This three rate well test example was presented by Odeh and Jones [14].

> "A three-hour drawdown test was conducted on a new well. The average flow rates during the first, the second, and the third hour were, respectively, 478.5, 319, and 159.5 reservoir bbl/day. The original reservoir pressure was 3,000 psi. The flowing bottom-hole pressure as a function of time is given in Table F.1. Calculate the average kh of the field."

Table F.1. Measured Data from Odeh and Jones' Three Rate Well Test Example

t (hours)	p_{wf} (psi)	q (STB/d)
0	3000	0
0.3	999	478.5
0.6	857	478.5
1	778.5	478.5
2	1378.5	319
2.3	2043	159.5
2.6	2067.5	159.5
3	2094	159.5

1. Interpolate Data Points at Equal Time Intervals. Linear interpolation was used to produce evenly spaced data with a time step of 1/3 of an hour. The pressure difference $p_i - p_{wf}$ was also calculated at each time step.

2. Deconvolve. The algorithm of Figure 3-1 on page 22 was used to deconvolved the evenly spaced data.

3. Log-log Diagnostic Plot. The log-log plot of the deconvolved pressure vs time shows that there are no wellbore storage effects (see Figure 4-15 on page 44). Radial flow is also evident from the deconvolved data.

4. Semi-log Plot. A semi-log plot of the well's deconvolved pressure vs time was used to find the slope. In the analysis of Odeh and Jones' data the fourth, fifth, seventh and eighth data points were ignored. Since Figure 4-15 does not indicate any wellbore storage, the trend set by the first three data points should be trusted. Since the trend set by the first three data points on the semi-log straight line of Figure 4-16 is continued by the sixth and nineth data points, these points should be used in the analysis and the fourth fifth, seventh and eight data points rejected. The reason that these four points do not follow the trend may be because the flow data was averaged over each hour, or because wellbore storage affects after each flow rate change were unquantified. A value of 460 psi/cycle is found from the semi-log straight line of Figure 4-16 on page 45.

5. Calculate Reservoir Parameters assuming [1] a reservoir fluid viscosity of 0.6 cp and using the equation

$$\hat{p}_{wf} = p_i + 162.6\frac{qB\mu}{kh}\left[\log\left(\frac{1688\phi\mu c_t r_w^2}{kt}\right) - 0.869s\right] \qquad \text{F.1}$$

with slope

$$m = 162.6\frac{qB\mu}{kh} = 460 \tag{F.2}$$

Rearranging to solve for permeability-thickness product,

$$kh = 162.6\frac{q_{ref}B\mu}{m} = 101.5mD - ft \tag{F.3}$$

The equation for calculating skin is

$$s = 1.151\left(\frac{p_i - \hat{p}_{1hr}}{m} - \log\left(\frac{k}{\phi\mu c_t r_w^2}\right) + 3.23\right) \tag{F.4}$$

From Figure 4-16 it is found that $\hat{p}_{1hr}$ is 778.5 psig. Lee [1] assumed that

$$\frac{k}{\phi\mu c_t r_w^2} = 4.81 \times 10^7 \tag{F.5}$$

Substituting this value into the above equation produces a skin of 0.43.

Permeability is similar to that reported by Odeh and Jones [14] who reported 103 md-ft. However, they did not report a skin value. Lee [1] analyzed the same data and reported a skin of 0.53.